Josephson junctions of two-dimensional time-reversal invariant superconductors: Signatures of the topological phase

Gabriel F. Rodríguez Ruiz,[1] Michael A. Rampp,[2,3] A. A. Aligia,[4] Joerg Schmalian,[2] and Liliana Arrachea[5]

[1]*Escuela de Ciencia y Tecnología and ICIFI, Universidad Nacional de San Martín, Av. 25 de Mayo y Francia, 1650 Buenos Aires, Argentina*

[2]*Institute for Theory of Condensed Matter, Karlsruhe Institute of Technology (KIT), 76131 Karlsruhe, Germany*

[3]*Max Planck Institute for the Physics of Complex Systems, 01187 Dresden, Germany*

[4]*Instituto de Nanociencia y Nanotecnología CNEA-CONICET, Centro Atómico Bariloche and Instituto Balseiro, 8400 Bariloche, Argentina*

[5]*Escuela de Ciencia y Tecnología and ICIFI, Universidad Nacional de San Martín-UNSAM, Av. 25 de Mayo y Francia, 1650 Buenos Aires, Argentina*

(Received 10 June 2022; revised 2 November 2022; accepted 8 November 2022; published 17 November 2022)

We determine the current-phase relation (CPR) of two-terminal configurations of Josephson junctions containing two-dimensional (2D) time-reversal invariant topological superconductors (TRITOPS), including TRITOPS-TRITOPS, as well as junctions between topological and nontopological superconductors (TRITOPS-S). We focus on wide junctions for which several channels intervene in the tunneling coupling. We derive effective Hamiltonians to describe the topological edge modes for different TRITOPS models, including Hamiltonians with p-wave pairing and Hamiltonians combining s-wave pairing with spin-orbit coupling. We also derive effective low-energy Hamiltonians to describe the Josephson junction. These can be solved analytically and explain the contribution of the edge states to the Josephson current as a function of the phase bias. We find that edge modes yield peculiar features to the CPR for both junction types. The primary effects occur for the response of the Majorana zero modes at half-flux quantum phase $\phi \approx \pi$ in TRITOPS-TRITOPS junctions and for integer flux quantum phase $\phi \approx 0$ for TRITOPS-S junctions, respectively. The former effect is particularly strong for two-component nematic superconductors. The second effect leads to a spontaneously broken time-reversal symmetry in the TRITOPS-S junction and to a breakdown of the bulk-boundary correspondence. We analyze in this case the role of the phase fluctuations. For weakly coupled junctions, we show that time-reversal symmetry is restored for large enough stiffness in these fluctuations.

DOI: 10.1103/PhysRevB.106.195415

I. INTRODUCTION

Topological superconductivity is among the most active research topics for some time now [1]. The topological superconductors are characterized by nontrivial topological quantum numbers in the bulk, which are usually accompanied by subgap excitations localized at the edges that behave as gapless Majorana fermions. Those have attracted great interest because of their potential application in quantum information processing [2–4].

The simplest model for topological superconductivity is Kitaev's model, which was formulated for spinless (or fully spin-polarized) fermions with p-wave pairing [2]. In one dimension (1D) the subgap states are Majorana bound states at zero energy that are localized at the ends of the superconducting wire. The latter are represented by operators satisfying $\gamma^\dagger = \gamma$ and $\gamma^2 = 1$. In two dimensions (2D) Majorana edge modes are massless and propagate along the edge in 1D channels satisfying $\eta_k^\dagger = \eta_{-k}$ and $\{\eta_k, \eta_{k'}\} = \delta_{k,k'}$. Such models guided the search for the topological phase in more realistic systems, where singlet superconductivity is the dominant type. A promising platform for the realization of topological superconductivity is based upon the combination of s-wave singlet superconductivity with spin-orbit coupling (SOC) and magnetic fields, which effectively generates p-wave superconductivity [5,6]. Several experiments in semiconducting wires with SOC in proximity with superconductors show features consistent with these ideas [7–11]. Another avenue to engineer a 1D topological superconductor is based on magnetic adatoms inducing subgap states in superconducting substrates [12–14]. Furthermore, the iron-based material FeSeTe, with intrinsic s-wave superconductivity and surface magnetism [15], as well as topological insulators in proximity with ordinary superconductors and magnetic islands [16,17] are also considered as a platform to realize Majorana states. Several results in this direction are reviewed in Refs. [18–21]. All the systems mentioned above rely on mechanisms breaking time-reversal symmetry. On the basis of symmetry analysis, it was recognized early on that other families of topological superconductors may exist [22]. Those preserving time-reversal symmetry are referred to as members of the *DIII-class* or TRITOPS (time-reversal symmetric topological superconductors). The key ingredient to realize this topological phase is the existence of two channels in which the pairing function have opposite signs [23]. Formally, a simple way to generate this effect is with two copies of Kitaev's model related by time-reversal symmetry [24–26] or by considering time-reversal-symmetric p-wave pairing [27]. Several theoretical proposals have been formulated in a number of systems. These include 2D and 3D models [11,23,28,29], as well as architectures of real systems like nanowires with Rashba spin-orbit coupling with proximitized d-wave [30] or extended s-wave

[31] configurations of two wires with spin-obit coupling, *s*-wave superconductivity and magnetic fields in arrangements globally preserving time-reversal symmetry [25,32–34], 2D topological insulators in proximity with superconductors [35–39], and thin films of iron-based superconductors [40]. As a consequence of the time-reversal symmetry, the edge modes of these topological systems appear in Kramers's pairs of Majorana modes. Their signatures can be identified in the noise spectrum and in the behavior of the Josephson current [32,41–52].

The hybridization between the topological edge states of topological superconductors in a Josephson junction leads to the formation of Andreev bound states. In 1D TRITOPS, the edge modes have zero energy and are localized at the end of the system. The corresponding Andreev bound states are characterized by symmetry-protected level crossings, which give rise to jumps in the current-phase relation (CPR) $J(\phi)$, ϕ being the phase bias at the junction. Such features depend on the structure of these modes, in particular, on the spin projection of their particle and hole components [45,49,53,54]. In 2D, the edge modes extend along the boundaries of the system. One of the goals of the present work is to analyze the structure of these modes, in particular, their dispersion relation and their spin structure.

In 2D, the characteristics of the Majorana edge modes are not universal but depend on the nature of the bulk. We show that they depend, in particular, on the details of the pairing mechanism and are also affected by the presence of the spin-orbit coupling. To properly analyze and compare these effects, we do not restrict ourselves to a single type of TRITOPS but consider models with and without spin-orbit coupling. We focus on two families of BCS models in 2D, which are representative of the different proposals reported in the literature: (a) *p-wave pairing*. Here our aim is to analyze the effect of spatial symmetry, which enables superconducting phases represented by one and two-dimensional order parameters. This is motivated by the observation of a nematic phase in the doped topological insulator $Cu_xBi_2Se_3$ [55,56], which has been suggested to be a TRITOPS with odd-parity superconducting pairing [28]. (b) *$s_\pm$-wave pairing in combination with SOC*, which are the ingredients of the TRITOPS platforms based on unconventional superconductors [31,40]. We derive effective Hamiltonians for the edge modes in each case which we compare with numerical results. These consist of 1D Dirac Hamiltonians describing the dynamics of the Kramers pairs of Majorana modes. The velocity of propagation of these modes as well as the structure of the spinors describing them are determined by the pairing mechanism of the bulk Hamiltonian and by the presence of the SOC.

The other goal of the present work is to analyze the impact that the structure of the edge modes have on the behavior of the CPR. We consider two types of Josephson junctions: (i) TRITOPS-TRITOPS and (ii) TRITOPS-S (S denotes a conventional superconductor). We derive effective low-energy Hamiltonians for these configurations, which can be solved analytically. The coupling of the edge modes in the junction generate ϕ-dependent mass terms in the Dirac Hamiltonians, which reveals the different nature of the junction. In the TRITOPS-TRITOPS case, the mass term is $\propto \cos(\phi/2)$, implying the opening of a gap in the spectrum of the topological Andreev modes close to $\phi = 0$. This mass term depends on the type of pairing and may have a complex structure which depends on the SOC. Instead, in the TRITOPS-S case, the mass generation is much more subtle. In this case the junction separates phases of different topology, and hence the bulk-boundary correspondence demands the edge to host gapless modes. This is reflected in the $\propto \sin(\phi)$ dependence of the mass term. This is a consequence of the fact that for $\phi = 0$ the Kramers' pair of edge modes remains robust under the coupling to the nontopological S system. However, as soon as the time-reversal symmetry is broken by a small ϕ, a gap develops in the corresponding Andreev spectrum. We show that this mechanism is very general and it takes place irrespective of the details of the pairing mechanism and the SOC. The outcome is a jump of the CPR at $\phi = 0$, implying an instability of the bulk-boundary correspondence as soon as the time-reversal-protecting symmetry is broken. The work is organized as follows. We introduce the models to be investigated in Sec. II. Section III is devoted to analyze the topological properties of the different models and to derive the effective Hamiltonians for the edge modes. We analyze the Josephson current in Sec. IV. Here we solve the problem numerically by diagonalizing exactly the lattice Hamiltonians and we also derive effective low-energy models based on the Josephson-tunneling coupling of the edge modes, which can be solved analytically. In all the cases we focus on junctions with many transverse channels that we analyze in the momentum space. Section V is devoted to analyze in detail the instability of the TRITOPS-S junction. Section VI contains a summary and conclusions, and some technical details are presented in Appendixes A–D.

II. MODELS FOR THE TRITOPS PHASE

We consider two different types of 2D models with BCS pairing defined in the square lattice and hosting a TRITOPS phase. (a) Models with *p*-wave pairing preserving time-reversal symmetry. The most studied case in the literature consists of two copies of the Kitaev model [23–25], where each copy has triplet pairing of fully polarized fermions. However, this is not the only possibility, since it is also possible to have triplet *p*-wave pairing between electrons with opposite spin orientation as it is well known in the context of He^3 [57,58]. Taking also into account the symmetry properties of the underlying lattice, we analyze the structure of the edge modes in the different irreducible representations of the *p*-wave pairing order parameter. This analysis is important in view of the nematic phase observed in the superconducting phase of the doped topological insulator $Cu_xBi_2Se_3$ [55,56]. Although this phase takes place in 3D, two-dimensional architectures based on this compound could inherit similar properties. We anticipate that, while the one-dimensional irreducible representations host dispersing edge modes, the edge modes of the two-dimensional one are dispersionless. (b) We also study a model where the pairing is of extended *s*-wave type in combination with SOC. Here we will see that the combination of these two ingredients effectively generates a *p*-wave-type pairing in the one-dimensional irreducible representations of the 2D lattice but with a spin structure of the edge modes affected by the SOC. In the forthcoming sections we

will analytically derive effective Hamiltonians for the edge modes and we will see how all these features lead to different signatures in the behavior of the CPR.

A. *p*-wave pairing

We consider the following Hamiltonian in the lattice $H = \frac{1}{2}\sum_{\mathbf{k}} \mathbf{c}_{\mathbf{k}}^{\dagger} H_{\mathbf{k}}^{p} \mathbf{c}_{\mathbf{k}}$, with $\mathbf{c}_{\mathbf{k}} = (c_{\mathbf{k},\uparrow}, c_{\mathbf{k},\downarrow}, c_{-\mathbf{k},\downarrow}^{\dagger}, -c_{-\mathbf{k},\uparrow}^{\dagger})^{T}$ and $\mathbf{k} = (k_x, k_y)$, while the Bogoliubov–de Gennes Hamiltonian matrix reads

$$H_{\mathbf{k}}^{p} = \xi_{\mathbf{k}} \tau^{z} \sigma^{0} + \tau^{x} \boldsymbol{\sigma} \cdot \boldsymbol{\Delta}_{\boldsymbol{k}}^{\alpha,\beta}. \tag{1}$$

The Pauli matrices $\tau^{x,y,z}$ and $\boldsymbol{\sigma} = (\sigma^{x}, \sigma^{y}, \sigma^{z})$ act, respectively, on the particle-hole and spin degrees of freedom, while τ^{0}, σ^{0} are 2×2 identity matrices. The dispersion relation is defined in terms of a hopping element t as $\varepsilon_{\mathbf{k}} = -2t(\cos k_x + \cos k_y)$; hence $\xi_{\mathbf{k}} = \varepsilon_{\mathbf{k}} - \mu$, being μ the chemical potential. Our results do not rely on the assumption of only nearest-neighbor hopping in $\varepsilon_{\mathbf{k}}$ and easily carry over to dispersions with further range hoppings. The p-wave pairing vector function, restricting to a $\mathbf{k}$ dependence with only linear terms in $\sin k_x$ and $\sin k_y$ and preserving time-reversal symmetry, reads

$$\boldsymbol{\Delta}_{\boldsymbol{k}}^{\alpha,\beta} = \Delta_x \sin k_x \, \mathbf{n}^{\alpha} + \Delta_y \sin k_y \, \mathbf{n}^{\beta}, \tag{2}$$

with (Δ_y, Δ_y) real. With the above restrictions, it is possible to build a pairing vector function for each of the irreducible representations of the point group D_{4h}:

$$\begin{aligned}
\boldsymbol{\Delta}_{\boldsymbol{k}}^{\mathrm{A}_{1u}} &= \Delta(\sin k_x \, \mathbf{n}^{x} + \sin k_y \, \mathbf{n}^{y}) \\
\boldsymbol{\Delta}_{\boldsymbol{k}}^{\mathrm{A}_{2u}} &= \Delta(\sin k_y \, \mathbf{n}^{x} - \sin k_x \, \mathbf{n}^{y}), \\
\boldsymbol{\Delta}_{\boldsymbol{k}}^{\mathrm{B}_{1u}} &= \Delta(\sin k_x \, \mathbf{n}^{x} - \sin k_y \, \mathbf{n}^{y}), \\
\boldsymbol{\Delta}_{\boldsymbol{k}}^{\mathrm{B}_{2u}} &= \Delta(\sin k_x \, \mathbf{n}^{y} + \sin k_y \, \mathbf{n}^{x}), \\
\boldsymbol{\Delta}_{\boldsymbol{k}}^{\mathrm{E}_{u}} &= \Delta(\sin k_x \pm \sin k_y) \, \mathbf{n}^{z},
\end{aligned} \tag{3}$$

$\mathbf{n}^{x,y,x}$ being unit vectors along the x, y, z directions. The A_{ju}, B_{ju}, $j = 1, 2$ are one-dimensional irreducible representations, while the E_{u} is two dimensional. For an intrinsic superconductor, the allowed values for the two components (Δ_x, Δ_y) are determined by the nonlinear, quartic terms of the Ginzburg-Landau expansion. The three options that result are, on the one hand, two solution proportional to either $(1, \pm 1)$ or $(1, 0)$ and $(0, 1)$. Those are nematic superconductors where the superconducting state breaks a rotation symmetry. On the other hand, there is the option proportional to $(1, \pm i)$ which breaks time-reversal symmetry and hence is not of the type discussed in this paper. Alternatively, superconductivity could be the consequence of a proximity effect to a substrate, in which case all the real combinations of (Δ_x, Δ_y) are consistent with the time-reversal symmetry. In addition, the edges of the samples are not necessarily aligned with the crystalline axes. We consider the particular real nematic phase with $\boldsymbol{\Delta}_{\boldsymbol{k}}^{\mathrm{E}_{u}}$ defined in Eq. (3), but we have checked that our conclusions hold for any other choice of (Δ_x, Δ_y).

B. $s_{\pm}$-wave pairing and SOC

The second type of model we will analyze is based on BCS pairing with s-wave symmetry in combination with spin-orbit coupling. We focus, in particular, on the model proposed by Zhang-Kane-Mele (ZKM) in Ref. [31], which is a BCS Hamiltonian with local Δ_0 plus extended Δ_1 s-wave pairing and Rashba spin-orbit coupling (SOC) λ. The Hamiltonian reads

$$H_{\mathbf{k}}^{\mathrm{ZKM}} = \xi_{\mathbf{k}} \tau^{z} \sigma^{0} + 2\lambda \tau^{z} (\sin k_x \sigma^{y} - \sin k_y \sigma^{x}) + \tau^{x} \sigma^{0} \Delta_{\mathbf{k}}. \tag{4}$$

The pairing potential has a local Δ_0 plus extended Δ_1 s-wave components, with $\Delta_{\mathbf{k}} = \Delta_0 + 2\Delta_1(\cos k_x + \cos k_y)$. This model hosts a topological phase for $|\mu - \varepsilon_0| < \varepsilon_1$, with $\varepsilon_0 = t\Delta_0/\Delta_1$ and $\varepsilon_1 = 2\lambda\sqrt{|\Delta_0/\Delta_1| - \Delta_0^2/(4\Delta_1^2)}$.

III. EFFECTIVE HAMILTONIANS FOR THE EDGE MODES

The TRITOPS phase is characterized by the existence of Kramers' pairs of Majorana edge modes. The aim of this section is to derive effective Hamiltonians to analytically describe the dynamics of these modes. This will be the starting point to analytically describe the Andreev spectra generated when these states are coupled in the Josephson junction. We focus on the two families of models previously introduced. For simplicity, we start the discussion with an analytic investigation of edge modes in the continuum limit. In the case of the ZKM model we must rely on an analytical solution of the lattice model in order to capture all the details introduced by the SOC. In all the cases we compare with the solution of the lattice Hamiltonian with a numerical approach.

A. *p*-wave model with A_{ju} and B_{ju} symmetry

A simple derivation of the effective Hamiltonian to describe the edge modes is possible by considering the continuum version of the Hamiltonian of Eq. (1). We start by analyzing the cases with $\Delta_{\mathbf{k}}^{\mathrm{A}_{1u}}$ and $\Delta_{\mathbf{k}}^{\mathrm{B}_{1u}}$, which correspond to

$$\mathcal{H}^{(1)} = \frac{1}{2} \int d^{2}x \, \Psi^{\dagger}(\mathbf{x}) \, H^{(1)} \, \Psi(\mathbf{x}), \tag{5}$$

with the Bogoliubov–de Gennes Hamiltonian,

$$H^{(1)} = \tau^{z} \sigma^{0} [\varepsilon_{\mathbf{p}} - \mu(x)] + \Delta \tau^{x} (p_x \sigma^{x} \pm p_y \sigma^{y}), \tag{6}$$

where $\pm$ corresponds to A_{1u} and B_{1u}, respectively. The Nambu field operators are defined as $\Psi(\mathbf{x}) = (\psi(\mathbf{x}), i\sigma^{y}\psi^{\dagger}(\mathbf{x}))^{T}$, $\psi(\mathbf{x}) = [\psi_{\uparrow}(\mathbf{x}), \psi_{\downarrow}(\mathbf{x})]^{T}$ being a spinor in spin space, while $\mathbf{x} = (x, y)$ and p_x, p_y denote the momentum in the x and y direction, respectively, with the dispersion relation $\varepsilon_{\mathbf{p}} = p^{2}/(2m)$.

The Hamiltonians for the edges along y read (see Appendix A for details)

$$H^{\nu} = \sum_{p_y \gtrless 0, \sigma} \mathrm{v}_{\nu,\sigma} \, p_y \eta_{\nu,p_y,\sigma}^{\dagger} \eta_{\nu,p_y,\sigma}, \tag{7}$$

where $\nu = l, r$ labels the left or right edges of a long ribbon along the y direction and $\mathrm{v}_{\nu,\sigma} = s_{\nu} s_{\sigma} \Delta$ is the velocity of propagation of the modes, with $s_{\uparrow} = -s_{\downarrow} = 1$. The corresponding Bogoliubov operators are

$$\eta_{\nu,p_y,\sigma} = \frac{e^{i s_{\nu} s_{\sigma} \pi/4}}{\sqrt{2}} (c_{\nu,p_y,\sigma} - i s_{\nu} s_{\sigma} c_{\nu,-p_y,\sigma}^{\dagger}), \tag{8}$$

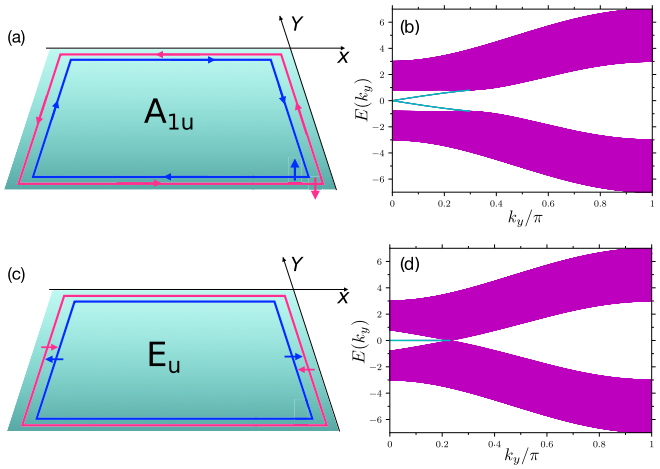

FIG. 1. Edge states and spectra for the topological phase of Hamiltonians with p-wave pairing. (a) and (b) correspond to the Hamiltonian of Eq. (1), with $\Delta_{\mathbf{k}}$ belonging to the one-dimensional irreducible representations of Eq. (3), while (c) and (d) to the two-dimensional representation E_u. Only A_{1u} (equal to A_{2u}) is shown. B_{1u} (equal to B_{2u}) has the same spin structure with opposite chiralities. The spectra are calculated for a system with open boundaries along the x direction and periodic boundary conditions along y (only $k_y \geqslant 0$ is shown). The edge states are indicated in light blue. These are twofold and fourfold degenerate in (b) and (d), respectively.

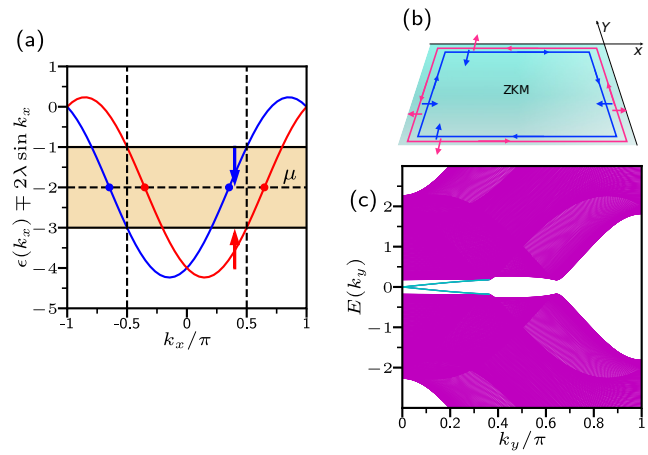

FIG. 2. (a) Bands of the Hamiltonian H^{ZKM} without pairing for $k_y = 0$. The yellow region indicates the range of values of μ within which the topological phase develops. The Fermi points indicated in dots are $-k_{F1}$, $-k_{F2}$, k_{F2}, k_{F1} (from left to right). (b) Sketch of the edge states for the continuum Hamiltonian. (c) Spectrum of H^{ZKM} with periodic boundary conditions along y and open boundary conditions along x in a system with $N_x = 200$. Parameters are $\Delta_0 = -2\Delta_1 = -0.4t$, $\lambda = 0.5t$, and $\mu = -2t$. The (doubly degenerate) edge states are indicated in light blue.

where $c_{\nu,p_y,\sigma}$ is the annihilation operator of a fermion with momentum p_y and spin σ at the edge ν. Notice that the Bogoliubov operators describing the edge modes, given in Eq. (8), satisfy the condition

$$\eta^{\dagger}_{\nu,p_y,\sigma} = \eta_{\nu,-p_y,\sigma}. \tag{9}$$

The solution for the edges along the x direction is similar, and the picture is consistent with two helical Majorana modes with associated opposite spin orientations circulating along the edges with opposite chiralities [see sketch of Fig. 1(a)]. The corresponding spectrum is presented in Fig. 1(b). The analysis of the representations A_{2u} and B_{2u} is completely analogous, and the solution is the same with an identical result.

B. p-wave model with E_u symmetry

We can proceed in a similar way as in Sec. III A. The Bogoliubov–de Gennes Hamiltonian for the continuum version in the present case reads

$$H^{\mathrm{E}_u} = \tau^z\sigma^0[\varepsilon_{\mathbf{p}} - \mu(x)] + \Delta\tau^x\sigma^z(p_x \pm p_y), \tag{10}$$

where, as before, we consider $\Delta > 0$, and the topological phase corresponds to $\mu > 0$. The calculation of the zero modes for $p_y = 0$ leads to a solution with identical structure as Eq. (A2), but with $\Lambda^{\nu}_{0,s}$ being a spinor that satisfies $\tau^y\sigma^z\Lambda^{\nu}_{0s} = s_\nu\Lambda^{\nu}_{0s}$, with $s_r = -s_l = 1$. Hence, $\Lambda^{\nu}_{0+} = \frac{1}{2}(1, 1, s_\nu i, -s_\nu i)^T$ and $\Lambda^{\nu}_{0-} = \frac{1}{2}(1, -1, s_\nu i, s_\nu i)^T$. Remarkably, the solution for $p_y \neq 0$ corresponds to evanescent modes, which is consistent with a flat band of zero modes localized at the edges. Therefore the edge modes are nondispersive. The sketch of these states along with the spectrum is shown in Figs. 1(c) and 1(d), respectively.

C. ZKM model

1. *Simplified continuum version*

To proceed as in the case of the p-wave BCS model, we define a low-energy continuum Hamiltonian for the lattice model defined in Eq. (4). The pairing potential of this model has a nodal surface for which $\Delta_k = 0$, which encloses the time-reversal-invariant point $\mathbf{k}_0 = (0, 0)$ for $\Delta_0/\Delta_1 < 0$, or $\mathbf{k}_0 = (\pi, \pi)$ for $\Delta_0/\Delta_1 > 0$ [31], and the topological phase develops when the Fermi energy approaches this surface. Due to the SOC, the system without pairing has two bands with different Fermi surfaces. The dispersion relation for $k_y = 0$ is shown in Fig. 2(a). The continuum model is obtained by linearizing this Hamiltonian with respect to the Fermi points of these two bands at the Fermi energy of the nodal surface of $\Delta_{\mathbf{k}}$. The procedure is explained in Appendix B. The effective low-energy Hamiltonian has p-wave pairing in the representations A_{ju} or B_{ju} along with SOC as an additional ingredient.

The Hamiltonian for the y edges reads

$$H^{\nu} = \sum_{p_y \geqslant 0, s=\pm} \mathrm{v}_s p_y \eta^{\dagger}_{p_y,s}\eta_{\nu,p_y,s}, \tag{11}$$

with $\mathrm{v}_s = s2\lambda$. Similar to the case of Eq. (8), the Bogoliubov operators describing the edge modes, given in Eq. (B6), satisfies the condition

$$\eta^{\dagger}_{\nu,p_y,s} = \eta_{\nu,-p_y,s}. \tag{12}$$

Notice, however, that the spin orientation is along the x direction in the present case. The solution for the edges running along the x direction is similar but with the spin orientation along y. The picture is consistent with two helical Majorana modes circulating along the edges with opposite chiralities and the spin texture shown in the sketch of Fig. 2(b). This

is consistent with the spectrum calculated by the exact diagonalization of Eq. (4), which is presented in Fig. 2(c).

2. General solution in the Lattice model

In the previous analysis we have linearized the Hamiltonian with respect to $\mathbf{k}$ points with one component of $\mathbf{k}_0$ kept fixed and the other component on the nodal lines of $\Delta_{\mathbf{k}}$, and we have calculated the corresponding effective Hamiltonians for the edge modes. For the sake of simplicity, we have neglected low-energy terms corresponding to linearizing the Hamiltonian with respect to other $\mathbf{k}$ values of the 2D Fermi surface. In those cases, the dispersion relation with respect to k_x keeping k_y fixed is similar to the one shown in Fig. 2(b) but with the orientation of the spin tilted with respect to z. In order to account for such more general context, we propose an ansatz for the description of the edge modes in terms of Bogoliubov operators with the structure of Eq. (B6) but with fermions having a tilted spin orientation. It reads

$$\eta_{v,k,s} = \frac{e^{-iss_v\pi/4}}{\sqrt{2}}(\tilde{f}_{v,k,s} + iss_v\tilde{f}^{\dagger}_{v,-k,s}), \quad s = \pm, \tag{13}$$

where k denotes the transverse direction to the finite-length ribbon, along which the edge localizes. The fermionic operators $\tilde{f}_{v,k,s}$ are

$$\begin{aligned}\tilde{f}_{v,k,+} &= e^{-i\delta_{v,k}}\left[\cos\left(\frac{\theta_{v,k}}{2}\right)f_{v,k,\uparrow} + e^{-i\varphi_{v,k}}\sin\left(\frac{\theta_{v,k}}{2}\right)f_{v,k,\downarrow}\right]\\ \tilde{f}_{v,k,-} &= e^{i\delta_{v,k}}\left[-e^{i\varphi_{v,k}}\sin\left(\frac{\theta_{v,k}}{2}\right)f_{v,k,\uparrow} + \cos\left(\frac{\theta_{v,k}}{2}\right)f_{v,k,\downarrow}\right],\end{aligned} \tag{14}$$

with $\theta_{v,k} = \theta_{v,-k}$, $\varphi_{v,k} = \varphi_{v,-k}$, $\delta_{v,k} = \delta_{v,-k}$, so that they are time-reversal partners, $\mathcal{T}\tilde{f}_{v,k,+}\mathcal{T}^{-1} = \tilde{f}_{v,-k,-}$, $\mathcal{T}\tilde{f}_{v,k,-}\mathcal{T}^{-1} = -\tilde{f}_{v,-k,+}$. These operators describe localized fermions at the v edge with spin-1/2 orientations along $\vec{n}_{v,k} = (\cos\theta_{v,k}\cos\varphi_{v,k}, \cos\theta_{v,k}\sin\varphi_{v,k}, \sin\theta_{v,k})$ in the coordinate system indicated in Fig. 2. For this reason, the fermions of Eq. (14) are basically the fermions $c_{v,p_y,s}$ of Eq. (B6) upon applying a SU(2) operation that tilts the spin from an orientation along the x direction to $\vec{n}_{v,k}$. Following the reasoning of Ref. [59], we notice that a SU(2) rotation in the fermions defining Majorana modes comes along with a change in the phases. For this reason we introduced the phase $\delta_{v,k}$ in Eq. (14), which, together with $\varphi_{v,k}, \theta_{v,k}$, define the generalized Bloch coordinates for each k value along the edge state.

This heuristic argument can be verified by following a similar procedure as in Refs. [60,61], modified to get analytical results as explained in Appendix C. Concretely, we consider the following lattice Hamiltonian:

$$\begin{aligned}H_k^{\mathrm{ZKM}} &= \sum_{j=1}^{L_x}\mathbf{c}^{\dagger}_{j,k}[\tau^z(\xi_k - 2\lambda\sin k\sigma^x) + \Delta_k\tau^x]\mathbf{c}_{j,k}\\ &+ \sum_{j=1}^{L_x-1}(\mathbf{c}^{\dagger}_{j,k}[\tau^z(-t - i\lambda\sigma^z) + \Delta_1\tau^x]\mathbf{c}_{j+1,k} + \mathrm{H.c.}),\end{aligned} \tag{15}$$

with $\mathbf{c}_{j,k} = (c_{j,k,\uparrow}, c_{j,k,\downarrow}, c^{\dagger}_{j,-k,\downarrow}, -c^{\dagger}_{j,-k,\uparrow})^T$, $\xi_k = -2t\cos k - \mu$, $\Delta_k = \Delta_0 + 2\Delta_1\cos k$. This corresponds to the Hamiltonian of Eq. (4) defined in a slab of L_x sites in the x direction and periodic boundary conditions in the transverse y direction (we are simplifying notation $k_y \equiv k$). The solution in the neighborhood of $k = k_{0,y}$ is given by Eqs. (13) and (14) with the angles $\theta_{v,k} = \pi/2$, $\varphi_{v,k} = -s_v\varphi_k$ and the phase $\delta_{v,k} = s_v\varphi_k/2$ with

$$s_l = -s_r = \mathrm{sgn}(\lambda\Delta_1). \tag{16}$$

Hence, all the angles and phases of the generalized Bloch coordinates can be expressed in the present case in terms of a single k-dependent phase φ_k. The fermionic operators $f_{v,k,\sigma}$ are related to the fermionic operators of the basis of the lattice model as follows:

$$\begin{aligned}f_{l,k,\sigma} &= \mathcal{N}_k\sum_{\ell=1}^{2}\alpha_{k,\ell,\sigma}\sum_{j=1}^{L_x}z^{j-1}_{k,\ell,\sigma}c_{kj\sigma},\\ f_{r,k,\sigma} &= \mathcal{N}_k\sum_{\ell=1}^{2}\overline{\alpha}_{k,\ell,\sigma}\sum_{j=1}^{L_x}\overline{z}^{L_x-j}_{k,\ell,\sigma}c_{kj\sigma},\end{aligned} \tag{17}$$

where $\mathcal{N}_k$ is a normalization factor, while $\alpha_{k,\ell,\uparrow} = \overline{\alpha}_{k,\ell,\downarrow} \equiv \alpha_{k,\ell} = \alpha_{-k,\ell}$ and $z_{k,\ell,\uparrow} = \overline{z}_{k,\ell,\downarrow} \equiv z_{k,\ell} = z_{-k,\ell}$ are complex coefficients which are determined by the open boundary conditions. The Hamiltonian for the edge modes reads

$$H_v = \sum_{k>0,s=\pm} s\varepsilon_{\lambda,k}\,\eta^{\dagger}_{v,k,s}\eta_{v,k,s}, \tag{18}$$

with

$$\varepsilon_{\lambda,k} = -2\rho_k\lambda\sin k. \tag{19}$$

The parameters ρ_k and φ_k are related to the parameters α_ℓ and z_j through

$$\rho_k e^{i\varphi_k} = \mathcal{N}_k^2\sum_{j=1}^{L_x}\left(\sum_{\ell=1}^{2}\alpha_{k,\ell}z^{j-1}_{k,\ell}\right)^2. \tag{20}$$

Importantly, $\rho_k \simeq \rho$, and $\varphi_k \simeq \varphi$ are approximately constant close to the Dirac point $k_{0,y}$, while ρ_k tends to zero as k significantly departs from this point. The structure of the edge modes corresponds to the sketch of Fig. 2, but with the spins tilted an angle φ with respect to the plane of the superconductor.

IV. JOSEPHSON JUNCTION AND CPR

Our goal now is to analyze of the impact on the Josephson current of the different types of edge states corresponding to the different platforms for realizing the TRITOPS phase. To this end, we consider two superconductors contacted in a Josephson junction. The hybridization of the states of the two superconductors leads to the development of Andreev states with energies below the superconducting gap. In the topological phase, these states are mainly originated by the hybridization between the edge states, which leads to peculiar features in the CPR. We analyze junctions between two TRITOPS as well as junctions between TRITOPS and an ordinary superconducting phase (S).

The Hamiltonian for the full system containing the two superconductors S_1, S_2 and the tunneling junction is expressed as $H = \sum_k H_k$ with

$$H_k = \sum_{\alpha=S_1,S_2} H_{\alpha,k} + H_{J,k}. \tag{21}$$

The Hamiltonian $H_{\alpha,k}$ corresponds to the TRITOPS Hamiltonian expressed in a slab of length N_x and periodic boundary conditions in the transverse direction, adopting a representation as in Eq. (15). The Hamiltonian for the tunneling junction is $H_J = \sum_k H_{J,k}$, with

$$H_{J,k} = t_J \sum_\sigma (e^{i\phi/2} c^\dagger_{S1,k,1,\sigma} c_{S2,k,1,\sigma} + \text{H.c.}), \tag{22}$$

where $c^\dagger_{S1,k,1,\sigma}$ ($c^\dagger_{S2,k,1,\sigma}$) creates an electron with spin σ in the superconductor S1 (S2) at the boundary contacting the junction with wave vector k in the transverse direction. The phase bias at the junction, $\phi = 2\pi\Phi/\Phi_0$, is defined by the total magnetic flux Φ, with $\Phi_0 = h/2e$ being the flux quantum. Our aim is to analyze features originated in the intrinsic properties of the topological edge states. For this reason we focus on Josephson junctions without spin-orbit effects. The latter usually introduce extra phases which affect the behavior of the Josephson current [54].

We calculate the Josephson current by diagonalizing exactly H_k and evaluating the energy of the ground state of this many-body Hamiltonian as [59,62]

$$E_0(k,\phi) = -\frac{1}{2}\sum_{s=\pm} \varepsilon_{k,s}(\phi), \qquad J(k,\phi) = \frac{2e}{\hbar}\frac{\partial E_0(k,\phi)}{\partial \phi}. \tag{23}$$

The energies $\varepsilon_{k,s}(\phi)$ are the negative single-particle energies of H_k. The total Josephson current as a function of ϕ (CPR) is simply calculated as $J(\phi) = \sum_k J_k(\phi)$. In all the cases we compare the exact numerical results with analytical ones that are obtained by substituting the exact Hamiltonians for the superconductors by effective Hamiltonians representing only the edge modes of the TRITOPS and/or a simplified version of the ordinary superconductor.

A. TRITOPS-TRITOPS junction

1. *p*-wave model

Results for the Josephson current for different k values in junctions between TRITOPS with p-wave pairing are shown in Fig. 3. The two panels of the figure illustrate the behavior of this quantity for the different representations of the p-wave pairing introduced before. The different colors distinguish the contributions associated to the hybridization of the edge modes from those corresponding to the hybridization of the continuum states. We can see the impact of the different structure of edge modes in the two cases.

The B_{1u} case is shown in the upper panel, and we recall that the spectrum of the edge modes has a linear dispersion relation. The contribution of the zero mode leads to a Josephson current which has a discontinuity at $\phi = \pi$ (see light-blue plot). This is the same behavior observed in topological superconducting wires and is a consequence of a level crossing of the Andreev states resulting from the hybridization of the Majorana zero modes [17,25,27,49,53]. Instead, the Josephson current is continuous as a function of ϕ for all the other edge modes with finite energy. Nevertheless, the observed behavior differs from the usual $\propto \sin(\phi)$ function of nontopological junctions (see violet plots). The latter behavior is observed only for k values associated to the continuum states (see red plots). We will see below that the Josephson coupling introduces a mass term in the effective Dirac Hamiltonian describing the free edge states, which explains the peculiar CPR of the propagating Majorana edge states. Identical results are obtained for the representations A_{2u} and B_{ju}, $j = 1, 2$. For the E_u case, where the edge modes form a flat band at zero energy, not only the $k = 0$ mode but all the edge modes show a discontinuity at $\phi = \pi$ (see lower panel of Fig. 3). The CPR is shown in Fig. 4 and is a superposition of all the k components.

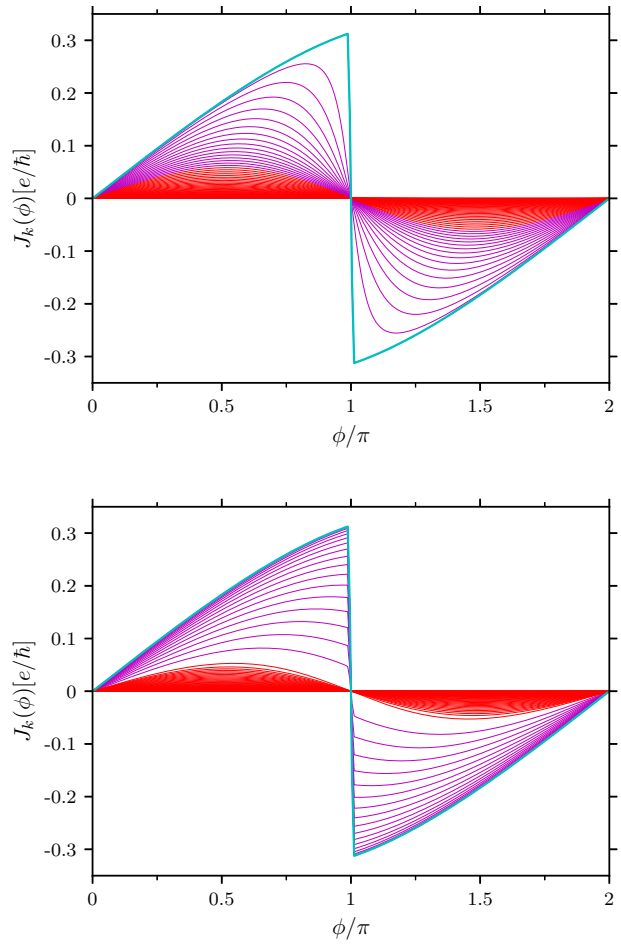

FIG. 3. k-resolved Josephson current (in units of $e/\hbar$) as a function of the phase difference in the topological phase for a junction of 2D topological superconductors with p-wave pairing calculated with numerical exact diagonalization. The upper and lower panels correspond to the representations A_{1u} (identical results are obtained for the A_{2u} and B_{ju}, $j = 1, 2$) and E_u, respectively. The plots in thick lines correspond to $k = 0$. Plots in violet correspond to the edge states, while the other k values are shown in red. The parameters are $t_J = \lambda = 0.5t$, $\Delta = t$, and $\mu = -3t$. A similar behavior is observed for other parameters within the topological phase ($-4t \leqslant \mu \leqslant 4t$)

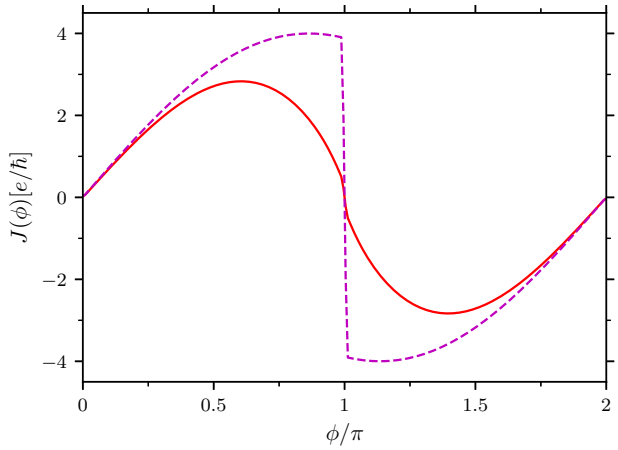

FIG. 4. Josephson current (in units of $e/\hbar$) as a function of the phase difference in the topological phase for a junction of 2D topological superconductors with p-wave pairing calculated by numerically diagonalizing the coupled lattice Hamiltonians. Solid and dashed lines correspond to the representation B_{1u} and E_u for $t_J = \lambda = 0.5t$, $\Delta = t$, and $\mu = -3t$.

In both types of junctions, the behavior of the Josephson current for k values associated to the edge states can be explained in terms a low-energy effective Hamiltonian for the junction [46,53,59], where we replace the fermionic operators for the TRITOPS' boundaries close to the junction $c_{S1,k,1,\sigma} \equiv c_{r,k,\sigma}$ and $c_{S2,k,1,\sigma} \equiv c_{l,k,\sigma}$ in Eq. (22) by their projections on the low-energy subgap excitations given by Eq. (8). Concretely, we perform the gauge transformation $\eta^\dagger_{\nu,k,\sigma} \to e^{is_\nu s_\sigma \pi/4}\eta^\dagger_{\nu,k,\sigma}$ and we substitute

$$c^\dagger_{\nu,k,\sigma} \simeq \frac{1}{\sqrt{2}}\eta^\dagger_{\nu,k,\sigma}, \qquad c^\dagger_{\nu,-k,\sigma} \simeq \frac{is_\nu s_\sigma}{\sqrt{2}}\eta_{\nu,k,\sigma}.$$

Introducing $\eta_{\nu,k} = (\eta_{\nu,k,\uparrow}, \eta_{\nu,k,\downarrow})^T$, for $k \geqslant 0$, we get the following effective Hamiltonian for the junction, obtained after adding the contributions of k and $-k$ in the original Hamiltonian:

$$H^{p-p}_{\text{eff},k} = t_\text{J}\cos(\phi/2)\eta^\dagger_{l,k}\eta_{r,k} + \text{H.c.} + \text{v}k\sum_\nu s_\nu \eta^\dagger_{\nu,k}\sigma^z\eta_{\nu,k}. \tag{24}$$

For the case of the E_u representation we have $\text{v} = 0$, and for the other representations we have $\text{v} = \pm\Delta$.

Defining the spinor $\eta_k = (\eta_{l,k,\uparrow}, \eta_{l,k,\downarrow}, \eta_{r,k,\uparrow}, \eta_{r,k,\downarrow})^T$, this effective Hamiltonian can be expressed as

$$H^{p-p}_{\text{eff},k} = \eta^\dagger_k[t_\text{J}\cos(\phi/2)\,\tilde\tau^x + \text{v}k\eta^\dagger_k\,\tilde\tau^z\sigma^z]\eta_k, \tag{25}$$

where the Pauli matrices $\tilde\tau^j$ act on the left-right degrees of freedom. We see that it has the structure of a Dirac Hamiltonian with a mass term $\propto \cos(\phi/2)$. The Hamiltonian of (25) can be diagonalized and has eigenenergies $\pm\varepsilon^{p-p}_k(\phi)$ with

$$\varepsilon^{p-p}_k(\phi) = \sqrt{(\text{v}k)^2 + t_\text{J}^2\cos^2(\phi/2)}, \tag{26}$$

which defines the Andreev spectrum. As a consequence of the dependence of the mass term with ϕ, a gap opens for arbitrary small ϕ. The derivative $\partial E_{k,-}/\partial\phi$ leads to a behavior of J_k that is perfectly consistent with the behavior reported in Fig. 3. For the E_u representation, the different amplitude of the discontinuity for different k values can be explained by taking into account the renormalization of t_J due to the k-dependent projection of the edge modes on the fermionic operators of the boundary in Eq. (24).

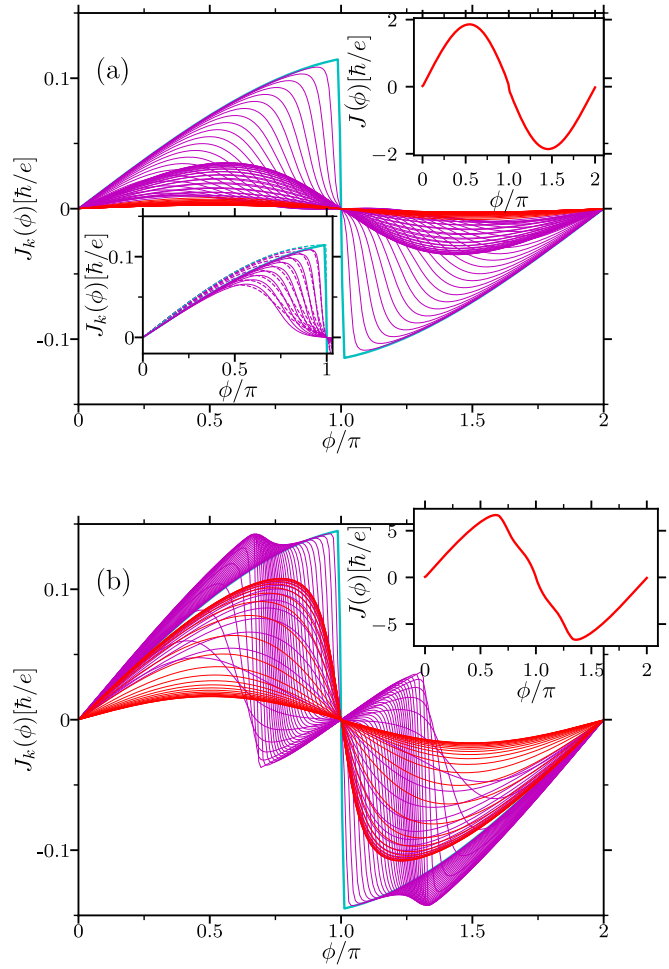

FIG. 5. (a) k-resolved Josephson current as a function of the phase difference in the topological phase for a junction of 2D topological superconductors with $t_J = t/2$, $\Delta_0 = 2\Delta_1$, and $\mu = \varepsilon_0$. The plot in thick lines corresponds to $k = \pi$. Plots in violet correspond to the edge states, while the other k values are shown in red. The upper insets show the total Josephson current and the effective Josephson current. The lower inset shows the comparison of the exact numerical solution with the prediction based on Eq. (35) with the effective parameters calculated with the exact solution as explained in Appendix C (dashed lines). (b) Same as top panel for $\Delta_0 = \Delta_1$ and $t_\text{J} = t$.

2. ZKM model

The Josephson current for the different k values as a function of the phase bias ϕ for the ZKM model is shown in Fig. 5. As in the previous section, we distinguish with different colors the contribution of the continuum states (red) and the edge modes (violet), highlighting the component of the zero modes corresponding to the time-reversal symmetric points $k_0 = 0, \pi$ (light blue). The latter mode presents the same type of discontinuity at $\phi = \pi$ observed in the p-wave models. We also observe the typical $\propto \sin(\phi)$ behavior in the contribution

of the states well inside the continuum. The behavior of the edge modes is more clearly distinguished for the parameters corresponding to the upper panel, and we will provide an analytical description below. The lower panel corresponds to parameters for which the superconducting gap is smaller. In this case, there is a strong hybridization between the topological edge states and those belonging to the quasiparticle continuum. We see interesting features, including several sign changes of $J_k(\phi)$ for such mixed states. The total CPR for different parameters is shown in the top insets of both panels.

In order to analyze the contributions of the edge states in the present case, we follow the same procedure as the previous section. Introducing the gauge transformation $\eta^\dagger_{\nu,k,s} \to e^{-is s_\nu \pi/4}\eta^\dagger_{\nu,k,s}$ we have

$$\tilde{f}_{\nu,k,s} = \frac{1}{\sqrt{2}}\eta_{\nu,k,s}, \quad \tilde{f}^\dagger_{\nu,-k,s} = -is s_\nu \frac{1}{\sqrt{2}}\eta_{\nu,k,s}, \tag{27}$$

with the fermionic operators defined in Eq. (14).

Therefore, assuming $\lambda\Delta_1 > 0$,

$$\begin{aligned} f_{\nu,k,\uparrow} &= \frac{e^{is_\nu\varphi_k/2}}{2}(\eta_{\nu,k,+} - \eta_{\nu,k,-}), \\ f_{\nu,k,\downarrow} &= \frac{e^{-is_\nu\varphi_k/2}}{2}(\eta_{\nu,k,+} + \eta_{\nu,k,-}), \\ f^\dagger_{\nu,-k,\uparrow} &= -is_\nu\frac{e^{-is_\nu\varphi_k/2}}{2}(\eta_{\nu,k,+} + \eta_{\nu,k,-}), \\ f^\dagger_{\nu,-k,\downarrow} &= -is_\nu\frac{e^{is_\nu\varphi_k/2}}{2}(\eta_{\nu,k,+} - \eta_{\nu,k,-}). \end{aligned} \tag{28}$$

Finally, we use the relation to the parameters of Eq. (17) corresponding to the wave function of the lattice Hamiltonian, which leads to

$$c^\dagger_{\nu,\pm k,\sigma} = \Omega_{\nu,k,\sigma} f^\dagger_{\nu,\pm k,\sigma}, \tag{29}$$

with

$$w_{l,k} = \Omega_{l,k,\uparrow} = \mathcal{N}_k \sum_{\ell=1}^{2} \alpha_{k,\ell} = \overline{\Omega}_{r,k,\uparrow} = \overline{\Omega}_{l,k,\downarrow} = \Omega_{r,k,\downarrow} = \overline{w}_{r,k}. \tag{30}$$

Substituting in Eq. (22), and assuming that the right edge of S1 is connected to the left edge of S2, leads to the effective Hamiltonian for the junction. Including the contribution of the free edge states described by Eq. (18) we get

$$\begin{aligned} H^{\mathrm{ZKM-ZKM}}_{\mathrm{eff},k} &= \cos(\phi/2)\sum_{s=\pm}[t_{1,k}\eta^\dagger_{r,k,s}\eta_{l,k,s} + it_{2,k}\eta^\dagger_{r,k,s}\eta_{l,k,-s} + \mathrm{H.c.}] \\ &\quad + \sum_{s=\pm} s\varepsilon_{\lambda,k}\,\eta^\dagger_{\nu,k,s}\eta_{\nu,k,s}, \end{aligned} \tag{31}$$

where $\varepsilon_{\lambda,k}$ is defined in Eq. (19), and we have introduced the definitions

$$t_{1,k} = t_\mathrm{J}\mathrm{Re}\left(w_k^2 e^{is_r\varphi_k}\right), \quad t_{2,k} = t_\mathrm{J}\mathrm{Im}\left(w_k^2 e^{is_r\varphi_k}\right). \tag{32}$$

The term in the first line of Eq. (31) describes the hybridization of the edge states through the Josephson-tunneling process, while the second one corresponds to the free edge states. In analogy to the case of the p-wave model, we can introduce the spinor $\eta_k = (\eta_{l,k,+}, \eta_{l,k,-}, \eta_{r,k,+}, \eta_{r,k,-})^T$, in terms of which the effective Hamiltonian reads

$$\begin{aligned} H^{\mathrm{ZKM-ZKM}}_{\mathrm{eff},k} &= \eta^\dagger_k[\cos(\phi/2)(t_{1,k}\tilde{\tau}^x + t_{2,k}\tilde{\tau}^y\sigma^x) \\ &\quad + \varepsilon_{\lambda,k}\sigma^z]\eta_k. \end{aligned} \tag{33}$$

We see that in the present case, the effective Hamiltonian for the coupled edge modes has the structure of the Dirac Hamiltonian as in the case of the p-wave model, but with two mass terms. Both mass terms are $\propto \cos(\phi/2)$, which implies the opening of a gap in the Andreev spectrum for arbitrary small ϕ. It is interesting to notice that, unlike the p-wave case, the two massive terms are k-dependent in this case. This is a consequence of the spin structure of the edge modes, which do not have a fixed direction in space but have a k-dependent tilt φ_k. The effective Hamiltonian can be diagonalized and has the following eigenenergies $\pm\varepsilon^{\mathrm{ZKM}}_{k,\pm}(\phi)$ with

$$\varepsilon^{\mathrm{ZKM}}_{k,\pm}(\phi) = \sqrt{[t_{1,k}\cos(\phi/2) \pm \varepsilon_{\lambda,k}]^2 + t_{2,k}^2\cos^2(\phi/2)}. \tag{34}$$

The calculation of the Josephson current for this effective Hamiltonian results in

$$\begin{aligned} J_{\mathrm{eff},k}(\phi) &= \frac{1}{2}t_{\mathrm{eff}}(\phi)\sin\left(\frac{\phi}{2}\right), \\ t_{\mathrm{eff}}(\phi) &= \frac{[t_{1,k}\cos(\phi/2) + \varepsilon_{\lambda,k}]t_{1,k} + t_{2,k}^2\cos(\phi/2)}{\varepsilon^{\mathrm{ZKM}}_{k,+}(\phi)} \\ &\quad + \frac{[t_{1,k}\cos(\phi/2) - \varepsilon_{\lambda,k}]t_{1,k} + t_{2,k}^2\cos(\phi/2)}{\varepsilon^{\mathrm{ZKM}}_{k,-}(\phi)}. \end{aligned} \tag{35}$$

For the time-reversal symmetric points $k_0 = 0, \pm\pi$, there is a level crossing in the spectrum because of which the ground-state energy $E_{0,\mathrm{eff}}(k,\phi)$ has a cusp and its derivative is discontinuous at $\phi = \pi$, which explains the jump in the Josephson current at this value of the phase. Other k values corresponding to the edge modes are semiquantitatively described by Eq. (35). An illustration is shown in the lower inset of Fig. 5(a), where the Josephson current calculated from exact diagonalization of the full lattice model is explicitly compared with the prediction of Eq. (35) based on the analytical calculation of the parameters w_k and φ_k from Eqs. (C10) and (C15). Although these parameters depend on k, close to the Dirac point, such dependence can be neglected. We see that the agreement is very good, and the slight quantitative mismatching can be understood by recalling that the analytical calculation introduces some approximations, namely, it treats λ perturbatively and also assumes strongly localized edge modes [see Eqs. (C14) and (C15)]. The plots of Fig. 5(b) correspond to parameters for which the superconducting gap is smaller. Under these conditions, the topological edge modes of each topological superconductor hybridize in the junction, not only with the topological edge states of the other superconductor but also with the nontopological states above the gap. As a consequence of this mixed hybridization, other features emerge, like the sign changes and a sawtooth-type behavior observed in these plots. This peculiar behavior can be qualitatively explained in terms of an effective Hamiltonian for the junction, which consists in adding a term representing the high-energy states to the effective low-energy Hamiltonian

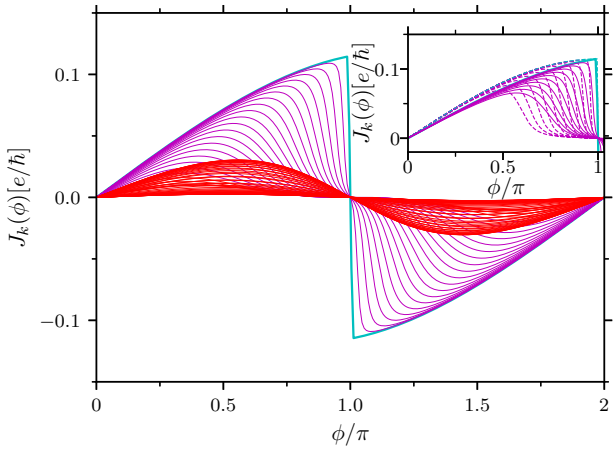

FIG. 6. k-resolved Josephson current for a junction tilted an angle $\beta = \pi/4$ respect to the xz plane with $t_J = t/2$, $\Delta_0 = 2\Delta_1$, $\mu = \epsilon_0$. Inset: Comparison with the effective model. Dashed lines correspond to Eq. (35), with the parameters defined in Eq. (36).

of Eq. (33). Such a procedure is similar to the one explained in the next section for the description of the TRITOPS-S junction.

We have considered so far junctions between TRITOPS with SOC oriented in the same direction. It is also interesting to consider a configuration where the two planes hosting the superconductors are tilted in an angle β around the z axis in the coordinate frame of Fig. 2(b). Introducing such a rotation in the Hamiltonian of S2 in H_k and in Eq. (22) leads to the k-resolved Josephson current shown in Fig. 6. We appreciate some different features for the k values corresponding to the edge modes, in comparison to Fig. 5(a), which has been calculated for the same parameters of the Hamiltonian in a junction without any tilt ($\beta = 0$). As before, the behavior of $J_k(\phi)$ for k belonging to the edge modes can be captured with a good degree of accuracy by the description provided by the effective Hamiltonian describing the Josephson-tunnel coupled edge modes. In the present case, this corresponds to Eq. (31) suitably modified to account for the tilt, which implies modifying the parameters to

$$t_{1,k} = t_J \mathrm{Re}\left(w_k^2 e^{-i(\varphi_k + \frac{\beta}{2})}\right), \quad t_{2,k} = t_J \mathrm{Im}\left(w_k^2 e^{-i(\varphi_k + \frac{\beta}{2})}\right). \quad (36)$$

This merely adds a shift $\beta/2$ to the tilt of the spins of the edge modes with respect to the plane of the superconductor. The corresponding contribution to the Josephson current calculated from this effective model is given by Eq. (35) with these modified parameters.

The net Josephson current, resulting from adding the contribution of all the transverse k channels, is shown in the upper right inset of Figs. 5(a) and 5(b). In the topological case, it shows a smooth but richer structure, which should be traced back to the maxima, minima, and crossings that take place for the k values corresponding to the edge states for these parameters.

B. TRITOPS-S junction

We now consider a Josephson junction between a TRITOPS and a nontopological superconductor. Concretely, we consider the Hamiltonian of Eqs. (21) and (22), with S1 being a BCS superconductor with only local pairing Δ_0. This corresponds to Eq. (4) with $\lambda = \Delta_1 = 0$. The results for the k-resolved Josephson current for S1 modeled by the three TRITOPS Hamiltonians studied in the previous sections are shown in Fig. 7.

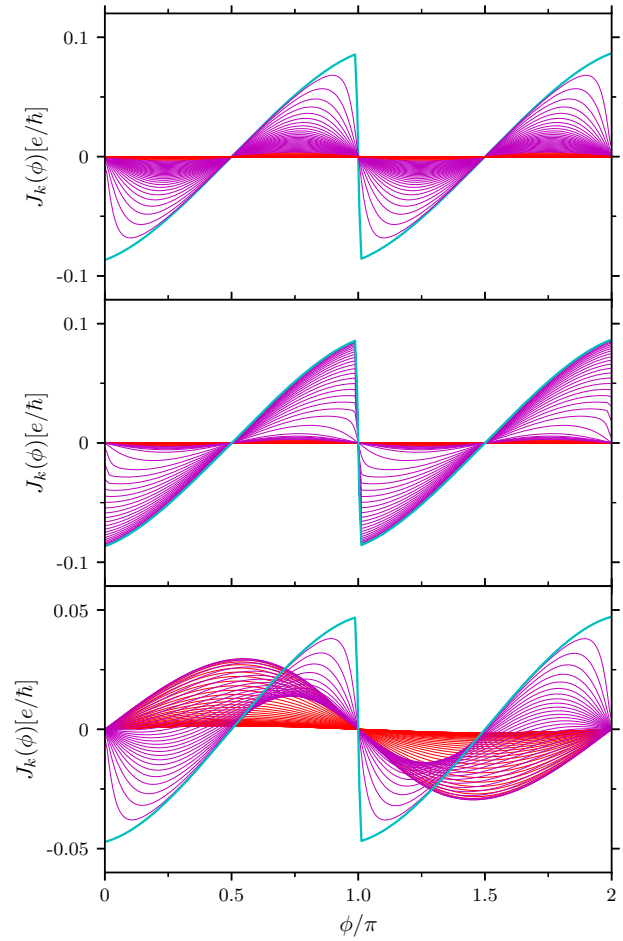

FIG. 7. k-resolved Josephson current as a function of the phase difference in the topological phase for a junction between a 2D topological superconductor with p-wave pairing (upper and middle panels) and a nontopological one with s-wave pairing. These panels correspond to the representation A_{1u} and E_u, respectively. The lower panel corresponds to a junction between the ZKM model and an ordinary superconductor (corresponding to $\Delta_1 = \lambda = 0$). The parameters are $t_J = \lambda = 0.5t$, $\Delta = \Delta_0 = 2\Delta_1 = 0.4t$, $\mu = \Delta_0/\Delta_1 t$.

The common pattern we can identify in these three configurations is the behavior of the k_0 component. It is characterized by three remarkable features, in striking contrast with the TRITOPS-TRITOPS junctions: (i) a sign change in $J_{k_0}(\phi)$, (ii) twice the periodicity in ϕ, and (iii) a discontinuous jump at $\phi = 0$. Such a peculiar behavior was discussed in the context of 1D systems in Refs. [23,41,49]. In the case of the E_u representation, these features are observed not only for k_0, but also for all the k values belonging to the (zero-energy) edge modes. A similar behavior was discussed in the framework of Josephson junctions between a superconductor with $d_{x^2-y^2}$ pairing and superconductors with s-wave pairing [63–65]. A jump in the CPR akin to the one observed in Fig. 7 is predicted when

the nodal line of the d-wave superconductor is perpendicular to the junction, as a consequence of zero modes in the interface. In our case, the existence of the zero modes is associated to the topological edge states. It is important to notice that this feature is, however, different from the so-called "anomalous Josephson effect" taking place when time-reversal symmetry is broken in the superconductor and/or in the junction at $\phi = 0$ [66–69]. In fact, as a consequence of the time-reversal symmetry, the CPR in the TRITOPS-S junction obeys $J(\phi = 0) = 0, \forall k$. A finite, albeit arbitrary small ϕ is necessary to induce the jump in $J_k(\phi)$ for k belonging to the zero-energy modes.

We can also derive an effective low-energy Hamiltonian for the TRITOPS-S junction. To this end, we consider the edge modes of the topological side, coupled to the high-energy quasiparticle excitations of the nontopological (S) one. In order to simplify the calculations, we neglect the free dispersion relation and we consider the following model for the S side:

$$H_{S,k} = \Delta_0(c^\dagger_{k,\uparrow}c^\dagger_{-k,\downarrow} + \text{H.c.}) = \sum_{s=\pm} s\Delta_0\, d^\dagger_{k,s}d_{k,s} + \text{constant}, \tag{37}$$

with $d_{k,s} = (c_{k,\uparrow} \pm c^\dagger_{-k,\downarrow})/\sqrt{2}$.

Considering the Hamiltonian of Eq. (8) for the edge states of the p-wave Hamiltonian expressed in the basis of the spinor $\eta_{v,k} = (\eta_{v,k,\uparrow}, \eta_{v,k,\downarrow})^T$ and integrating out the degrees of freedom of the ordinary superconductor in the second order of perturbation theory in the tunneling coupling t_J, we get

$$H_k^{p-\text{S,eff}} = \eta_k^\dagger\left[\tilde{\varepsilon}_k^p\sigma^z + m^p\sin(\phi)\sigma^y\right]\eta_k \tag{38}$$

with

$$\tilde{\varepsilon}_k^p = \text{v}ks_v, \qquad m^p = -|t_J|^2/\Delta_0. \tag{39}$$

For the case of the ZKM model, we can consider the projections on the edge modes of the fermionic operators at the end of the TRITOPS by using Eqs. (27), (28), and (29) and integrate out the fermions of the S side in a similar way as before. This leads to the following effective Hamiltonian for the junction expressed in the basis of the spinor $\eta_k = (\eta_{v,k,+}, \eta_{v,k,-})^T$ (see Appendix D for details):

$$H_{v,k}^{\text{ZKM}-\text{S,eff}} = \eta_k^\dagger\left[\tilde{\varepsilon}^{\text{ZKM}}\sigma^z + m_k^{\text{ZKM}}\sin(\phi)\sigma^x\right]\eta_k, \tag{40}$$

where we adopt the same notation as in Sec. IV A 2 and we have introduced

$$\tilde{\varepsilon}_k^{\text{ZKM}} = \varepsilon_{\lambda,k}(1 - m^{\text{ZKM}}/\Delta_0), \qquad m^{\text{ZKM}} = 2s_v t_J^2|w_k|^2/\Delta_0. \tag{41}$$

The diagonalization of the two Hamiltonians defined in Eqs. (38) and (40) for the TRITOPS-S junction leads to the eigenstates $\pm\varepsilon_k^{\text{T}-\text{S}}(\phi)$ with

$$\varepsilon_k^{\text{T}-\text{S}}(\phi) = \sqrt{(m^{\text{ZKM}})^2\sin^2(\phi) + \tilde{\varepsilon}_k^2}, \tag{42}$$

with the parameters defined in Eqs. (39) and (41) for the p-wave and ZKM Hamiltonians for the TRITOPS, respectively. This leads to the many-body ground-state energy $E_0(\phi) \equiv -\varepsilon_k^{\text{T}-\text{S}}(\phi)$. Hence, the Josephson CPR is given by

$$J_{\text{eff},k}(\phi) = -\frac{1}{2\varepsilon_k^{\text{T}-\text{S}}(\phi)}(m^{\text{ZKM}})^2\sin(2\phi). \tag{43}$$

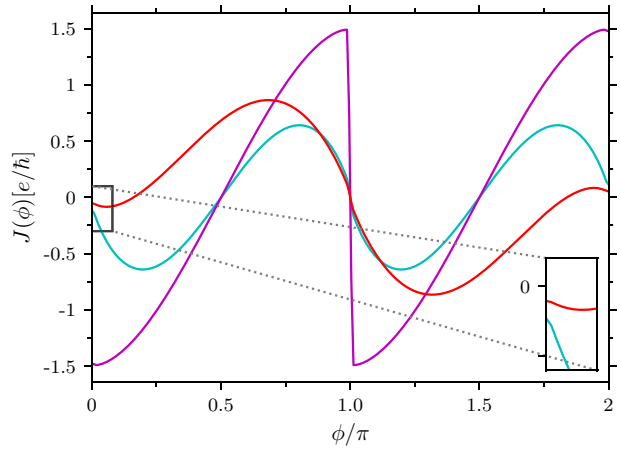

FIG. 8. Total Josephson current as a function of the phase difference in the topological phase for a junction between a 2D topological superconductor and a nontopological one with s-wave pairing. Light blue, violet, and red colors correspond to the A_{1u}, E_u, and ZKM models, respectively.

This analytical expression is in full agreement with the behavior of the Josephson current for k corresponding to the edge states shown in Fig. 7. In the case of the p-wave pairing within the E_u representation, which is shown in the middle panel, all the k components close to the Dirac point have a jump at $\phi = 0$ because the edge channels are dispersionless, and hence $\tilde{\varepsilon}_k = 0$ in Eq. (42).

To finalize, we show in Fig. 8 the total CPR obtained by adding all the k components for the three models. We see that all three cases are characterized by a jump at $\phi = 0, \mod(\pi)$. As expected, the amplitude of this feature is much more pronounced in the case of the E_u-type p-wave pairing.

V. INSTABILITIES AND BULK-BOUNDARY CORRESPONDENCE

In this section we discuss how our findings are related to the expectations that follow from the bulk-boundary correspondence. We will see that the behavior at TRITOPS-TRITOPS junctions is fully in line with the bulk-boundary correspondence. The junction separates two topologically nontrivial systems. Hence states in the junction area should be gapped. The tunneling term between two TRITOPSs must therefore induce a gap of the edge states of both topological superconductors. By the same logic one would expect massless states at the TRITOPS-S junction, as it separates a topologically trivial and nontrivial state. However, our results imply that TRITOPS-S junctions violate the bulk-boundary principle. We will argue that this is a consequence of the spontaneously broken time-reversal symmetry in the TRITOPS-S junction itself. With the protecting symmetry spontaneously broken at the edge, edge states become massive. We expect this to be a fully generic feature of TRITOPS-S junctions.

The low-energy states of both junctions can be described in terms of a Majorana spinor with Hamiltonian

$$H_{\text{edge}} = vp\alpha + m(\phi)v^2\beta. \tag{44}$$

For the TRITOPS-TRITOPS junction we have a four-component Majorana spinor. We focus on the p-wave case Eq. (40), for which $\alpha = \tilde{\tau}^z\sigma^z$ and $\beta = \tilde{\tau}^x$. In addition, the fermion mass depends on the relative phase according to $m(\phi) = m_0 \cos(\phi/2)$, where m_0 is linearly proportional to the tunneling matrix element t_J. In distinction, at the TRITOPS-S junction we have a two-component Majorana spinor with $\alpha = \sigma^z$, $\beta = \sigma^x$. The most crucial difference is the phase dependence of the mass $m(\phi) = m_0 \sin\phi$, where $m_0 \propto t_J^2/\Delta_0$ with pairing gap Δ_0 of the topologically trivial superconductor.

So far, we have considered the phase bias of the junction as a parameter that is fixed by external conditions, like implementing the junction in a ring-shape structure threaded by a magnetic flux. We now consider the junction regarding ϕ as an internal degree of freedom in order to analyze the stability close to $\phi = 0$. The usual phase dependence of the Josephson energy is

$$E_{J,0}(\phi) = \frac{1}{2\lambda_J^2}(1 - \cos\phi), \tag{45}$$

which yields an equilibrium phase $\phi^* = 0\,\mathrm{mod}(2\pi)$. Equation (45) is the result of tunneling due to states above the bulk pairing gap, just like in any other superconductor. Using this value for the equilibrium phase difference ϕ^* and inserting in the two mass-phase relations for the two junction types, edge states are massive for TRITOPS-TRITOPS junctions $[\cos(\phi^*/2) \neq 0]$ and massless for TRITOPS-S junctions $[\sin(\phi^*) = 0]$. This is in line with the expectation that follows from the bulk-boundary correspondence.

It is, however, important to analyze the impact of the edge states on the current-phase relation, i.e., to properly include the edge-state contribution to the Josephson energy:

$$E_J(\phi) = E_{J,0}(\phi) + \delta E_J(\phi). \tag{46}$$

Here,

$$\delta E_J(\phi) = \langle H_{\mathrm{edge}}\rangle_\phi - \langle H_{\mathrm{edge}}\rangle_{\phi=0} \tag{47}$$

is the phase-dependent expectation value of the energy due to edge modes. We made the assumption that the phase stays constant in space along the junction, an assumption that we will relax below.

In order to determine $\delta E_J(\phi)$, we integrate out the edge-state fermions. To justify this we assume and check later for consistency that the fermion mass is finite. It follows from H_{edge} of Eq. (44) that

$$\delta E_J(\phi) = -\frac{v}{8\pi} m(\phi)^2 \log\left(\frac{\Lambda^2}{m(\phi)^2}\right). \tag{48}$$

Here Λ is the high-energy cutoff.

Let us first comment on the impact of edge modes on the current-phase relation of TRITOPS-TRITOPS junctions. If we use $m(\phi) = m_0 \cos(\phi/2)$ in Eq. (48), the minimum in $E_J(\phi)$ continues to be at $\phi = 0\,\mathrm{mod}(2\pi)$ and the edge modes are indeed massive $m(\phi^*) = m_0 \neq 0$, fully consistent with the bulk-boundary correspondence. Only near $\phi = \pi$, where the fermion mass changes sign, do we find a singular behavior for the current:

$$J(\phi) \sim -\log\left(\frac{\Lambda^2}{m_0^2(\phi-\pi)^2}\right)(\phi - \pi). \tag{49}$$

This is the main effect of edge modes for TRITOPS-TRITOPS junctions.

More dramatic behavior occurs at the TRITOPS-S junction. With $m(\phi) = m_0 \sin\phi$, one easily finds that the singular logarithmic dependence near $\phi = 0$ implies that the minimum in $E_J(\phi)$ is always shifted to a finite phase ϕ^*, yielding a finite fermion mass, which corresponds to broken chiral symmetry. Using $C = \mathcal{P}\mathcal{T}$ for the chiral, parity, and time-reversal symmetries, we see that broken C with intact $\mathcal{P}$ breaks the time-reversal symmetry, as expected for a junction with nontrivial phase difference $\phi \neq 0, \pi$. Clearly the bulk-boundary correspondence does not apply.

We conclude that the edge modes at the junction between a TRITOPS and a conventional superconductor are not gapless but massive, which is closely connected to a finite equilibrium phase difference at the junction. The bulk-boundary correspondence at the edge is invalidated, as the gapless modes are unstable against an infinitesimal Josephson coupling. The protecting time-reversal symmetry is broken at the junction as a consequence of the phase-edge mode coupling.

Other physical effects may play a role. Particularly interesting is the role of phase fluctuations, which could induce mechanisms tending to restore the broken time-reversal symmetry in the TRITOPS-S junction. Another interesting effect that could take place in the coupled dynamics of the edge states and the phase fluctuations is the emergence of Majorana zero modes that are tied to solitonic phase slips. Those localized zero modes are expected for both junction types. All these phenomena are worthy of being analyzed in combination with capacitive electron-electron interactions in the junction. The starting points to this goal are the effective Hamiltonians of Eqs. (25), (33), (38), and (40), which we have derived for the different junctions, suitable for extension to address these other effects.

VI. CONCLUSIONS

We have studied different models for two-dimensional time-reversal symmetric topological superconductors (TRITOPS), with and without spin-orbit coupling. To this end, we have derived effective Hamiltonians for the edge modes and shown that their spectrum and spin texture strongly depend on the point-group symmetry of the superconducting pairing as well as on the spin-orbit coupling.

We then analyzed wide Josephson junctions between two topological superconductors (TRITOPS-TRITOPS), as well between a topological superconductor and an ordinary s-wave superconductor (TRITOPS-S). The discontinuous current-phase relation near $\phi = \pi$, known from junctions between two one-dimensional topological superconductors, continues to be visible in our wide TRITOPS-TRITOPS junctions. It is particularly pronounced in the two-component, nematic superconductors, where edge modes are nondispersive. This result follows not only from our approximate continuum's theory but is equally present in the full numerical solution of the lattice version. Singular behavior near $\phi = \pi$ is, however, also present in other junctions between two TRITOPSs, albeit weaker given the edge-state dispersion. This behavior is caused by vanishing mass of the edge modes at $\phi = \pi$.

The behavior is rather different in TRITOPS-S junctions between a time-reversal symmetric topological and a topologically trivial superconductor. Now the edge-mode gap vanishes for $\phi = 0$, and minimization of the energy leads to a finite but small ϕ leading to time-reversal symmetry breaking in the edge. This endows the edge modes with a mass and generates an unexpected jump in the Josephson current.

These results provide useful hints in the experimental search of the TRITOPS phase. In addition, the effective Hamiltonians for the different junctions we have derived in the present work are the foundation stones to investigate several other interesting phenomena that may take place in Josephson junctions with time-reversal symmetric topological superconductors and can be extended to analyze the effect of phase fluctuations, the generation of solitonic modes, and charging effects.

ACKNOWLEDGMENTS

We are grateful to Dmitriy S. Shapiro and Alexander Shnirman for helpful discussions. We acknowledge financial support provided by PICT 2017-2726 and PICT 2018-01546 of the FonCyT, and CONICET Argentina. We also thank the SPUK Collaboration (J.S. and L.A.) and the Alexander von Humboldt Foundation (L.A.) for support.

APPENDIX A: DETAILS OF THE DERIVATION OF THE EDGE STATES OF THE *p*-WAVE MODEL

We assume $\Delta > 0$, and the topological phase corresponds to $\mu > 0$. We focus on an edge intersecting the horizontal axis at the $x = 0$ of a slab of infinite length along the y direction. To analyze the right/left edge, we consider a domain wall of the form $\mu^{r/l}(x) = \mp \mathrm{sgn}(x)|\mu_0|$, which corresponds to the topological phase in the region with $x < 0\,/\,x > 0$, respectively.

For $p_y = 0$, there exists a Kramer's pair of Majorana zero modes, which can be calculated from the solution of

$$\{-\mu^{\nu}(x)\tau^z\sigma^0 + \Delta\tau^x(-i\partial_x\sigma^x)\}\Phi^{\nu}_0(x) = 0, \tag{A1}$$

where we have neglected, for simplicity, the dispersion relation. The solutions are

$$\Phi^{\nu}_{0,s}(x) = g^{\nu}(x)\Lambda^{\nu}_{0s}, \qquad g^{\nu}(x) = g_0 e^{s_{\nu}\int_0^x dx' \frac{\mu^{\nu}(x')}{\Delta}}, \tag{A2}$$

with $\Lambda^{\nu}_{0,s}$ being a spinor that satisfies $\tau^y\sigma^x\Lambda^{\nu}_{0s} = s_{\nu}\Lambda^{\nu}_{0s}$, with $s_r = -s_l = 1$ and $s = \pm$. Hence, $\Lambda^{\nu}_{0s} = \frac{1}{2}(1, s, s_{\nu}si, s_{\nu}i)^T$. For finite p_y we look for solutions of the form

$$\Psi(\mathbf{x}, t) = \sum_{p_y>0} e^{-iE^{\nu}_{p_y}t}\left(\Phi^{\nu}_{p_y}(\mathbf{x})\eta_{\nu,p_y} + C\mathcal{T}\Phi^{\nu}_{p_y}(\mathbf{x})\eta^{\dagger}_{\nu,p_y}\right), \tag{A3}$$

with $C\mathcal{T} \equiv -i\tau^y i\sigma^y\mathcal{K}$, where C is the charge conjugation, $\mathcal{T}$ is the time-reversal operator in Nambu space, $\mathcal{K}$ is complex conjugation, and the Bogoliubov operator is $\eta_{\nu,p_y} = \int d^2x\Phi^{\nu\dagger}_{p_y}(\mathbf{x})\Psi(\mathbf{x})$. Hence, we must solve

$$\{-\mu^{\nu}(x)\tau^z\sigma^0 + \Delta\tau^x(-i\partial_x\sigma^x \mp i\partial_y\sigma^y)\}\Phi^{\nu}_{p_y}(\mathbf{x}) = E^{\nu}_{p_y}\Phi^{\nu}_{p_y}(\mathbf{x}). \tag{A4}$$

We find two degenerate solutions, which we label with $\sigma = \uparrow, \downarrow$ for each p_y. The eigenenergies are

$$E^{\nu}_{p_y,\sigma} = \pm \mathrm{v}_{\nu,\sigma}\, p_y\,, \tag{A5}$$

with $\mathrm{v}_{\nu,\sigma} = s_{\nu}s_{\sigma}\Delta$, with $s_{\uparrow} = -s_{\downarrow} = 1$. The eigenfunctions are

$$\Phi^{\nu}_{p_y,\sigma}(x, y) = g^{\nu}(x)e^{is_{\nu}s_{\sigma}\pi/4}e^{ip_y y}\Lambda^{\nu}_{0,\sigma},$$
$$\Lambda^{\nu}_{0,\sigma} = \frac{\left(\Lambda^{\nu}_{0,+} + s_{\sigma}\Lambda^{\nu}_{0,-}\right)}{\sqrt{2}}. \tag{A6}$$

The corresponding Bogoliubov operators are

$$\eta_{\nu,p_y,\sigma} = \frac{e^{is_{\nu}s_{\sigma}\pi/4}}{\sqrt{2}}(c_{\nu,p_y,\sigma} - is_{\nu}s_{\sigma}c^{\dagger}_{\nu,-p_y,\sigma}). \tag{A7}$$

APPENDIX B: DERIVATION OF AN APPROXIMATE CONTINUUM HAMILTONIAN FOR THE ZKM MODEL

We find it convenient to transform the Hamiltonian of Eq. (4) by means of a rotation $R = e^{-i\pi/4\sigma^x}$ in the spin degrees of freedom, which transforms $\sigma^y \to \sigma^z$. The derivation of the continuum Hamiltonian is particularly simple for $\Delta_0 = \pm 2\Delta_1$ and we shall focus on $\lambda,\ \Delta_1 > 0$. Let us assume, for concreteness, the case with $\Delta_0 = -2\Delta_1,\ \lambda > 0$, and $k_y = 0$, in which case the nodal surface crosses at the nodal points $(\pm\pi/2, 0)$, and the two bands have a well-defined z component of the spin $\pm\,1/2$.

For $|\mu + 2t| \leqslant 2\lambda$, there are four Fermi points in the k_x axis [see Fig. 2(a)]. We call them $\pm k^F_1, \pm k^F_2$, with k^F_1 and k^F_2 belonging to the different branches $\uparrow, \downarrow$, respectively. Hence, linearizing with respect to the Fermi points, the spectrum without pairing has right and left movers with $\uparrow, \downarrow$ z component of spin. Projecting the pairing potential on the Fermi points and expanding with respect to the points $\pm\pi/2$, which are precisely the nodal points of this potential, we have the following low-energy Hamiltonian

$$H^{k_y=0}_{\mathbf{p}} = -\delta\mu\tau^z\sigma^0 + 2\Delta_1 p_x\tau^x\sigma^z + 2\lambda p_y\tau^z\sigma^x, \tag{B1}$$

which is defined in the basis of the spinor $(c_{k^F_1,\uparrow}, c_{k^F_2,\downarrow}, c^{\dagger}_{-k^F_1,\downarrow}, -c^{\dagger}_{-k^F_2,\uparrow})^T$ with $|p_x| = k^F_1 - \pi/2 = \pi/2 - k^F_2$, $p_y = k_y$, $\mathbf{p} = (p_x, p_y)$, and $\delta\mu = \mu + 2t - 2\lambda$.

We can repeat the argument along k_y for $k_x = 0$. The difference is that the two bands represented in Fig. 2(a) have spin components along the x direction instead of z. The resulting Hamiltonian is

$$H^{k_x=0}_{\mathbf{p}} = \delta\mu\tau^z\sigma^0 + 2\Delta_1 p_y\tau^x\sigma^x - 2\lambda p_x\tau^z\sigma^z, \tag{B2}$$

with $p_y = k_y \mp \pi/2$, $p_x = k_x$. Furthermore, a similar reasoning can be followed for the case with $\Delta_0 = 2\Delta_1$ for $|\mu - 2t| \leqslant 2\lambda$ and the same values of the other parameters. For simplicity, we have neglected the momentum dependence of the dispersion relation of the two bands without pairing at the Fermi energy.

We now consider the Hamiltonian $H^{k_y=0}_{\mathbf{p}}$ given by Eq. (B1) to derive the wave function and the effective Hamiltonian for the edge states along the y direction. The structure of the solution for the case $p_y = 0$ is identical to Eq. (A1). In turn, as pointed out in the previous section, this solution has an identical structure as Eq. (A2), but $\Lambda^{\nu}_{0,\sigma}$ is now a spinor that satisfies $\tau^y\sigma^z\Lambda^{\nu}_{0\sigma} = s_{\nu}\Lambda^{\nu}_{0\sigma}$, with $s_r = -s_l = 1$ and $\sigma = \uparrow, \downarrow$. Hence, $\Lambda^{\nu}_{0\uparrow} = (1, 0, s_{\nu}i, 0)$ and $\Lambda^{\nu}_{0\downarrow} = (0, 1, 0, -s_{\nu}i)$. For $p_y \neq 0$, we consider a field operator with the structure of

Eq. (A3), where the spinors should satisfy

$$\{-\mu^{\nu}(x)\tau^{z}\sigma^{0}+2\Delta_{1}\tau^{x}(-i\partial_{x}\sigma^{z})+2\lambda p_{y}\tau^{z}\sigma^{x}\}\Phi^{\nu}_{p_{y}}(x) = E^{\nu}_{p_{y}}\Phi^{\nu}_{p_{y}}(x). \tag{B3}$$

We find two degenerate solutions, which we label with $s = +, -$ for each p_y. The eigenenergies are

$$E^{\nu}_{p_{y},s} = \mathrm{v}_{s}p_{y} \tag{B4}$$

with $\mathrm{v}_s = s2\lambda$. The eigenfunctions are

$$\Phi^{\nu}_{p_{y},s}(x,z) = g^{\nu}(x)e^{-is s_{\nu}\pi/4}e^{ip_{y}y}\Lambda^{\nu}_{0,s},$$
$$\Lambda^{\nu}_{0,s} = \frac{\left(\Lambda^{\nu}_{0,\uparrow}+s\Lambda^{\nu}_{0,\downarrow}\right)}{\sqrt{2}}, \tag{B5}$$

and the corresponding Bogoliubov operators can be expressed as

$$\eta_{\nu,p_{y},s} = \frac{e^{-is s_{\nu}\pi/4}}{\sqrt{2}}(c_{\nu,p_{y},s}+is s_{\nu}c^{\dagger}_{\nu,-p_{y},s}),$$
$$c_{\nu,p_{y},s} = \frac{1}{\sqrt{2}}(c_{\nu,p_{y},\uparrow}+sc_{\nu,p_{y},\downarrow}), \qquad \Delta_{0}/\Delta_{1}<0. \tag{B6}$$

The corresponding effective Hamiltonians for the edges are given in Eq. (11).

For the case with $\Delta_0/\Delta_1 > 0$, we can follow a similar approach, taking into account that the expansion leading to the effective continuum Hamiltonian must be done with respect to $\mathbf{k}_0 = (\pi, \pi)$. In such a case, we would get for $H^{k_y=\pi}_{\mathbf{p}}$, with $p_x = k_x \pm \pi/2$, $p_y = k_y - \pi$, and $H^{k_x=\pi}_{\mathbf{p}}$,with $p_x = k_x - \pi$, $p_y = k_y \pm \pi/2$, expressions like those of Eqs. (B1) and (B2) but with opposite sign of the pairing term.

APPENDIX C: EXACT SOLUTION OF THE ZKM HAMILTONIAN FOR A TRANSVERSE CHANNEL

We consider the ZKM model in a ribbon of finite length N_x along the x direction and periodic boundary conditions in the transverse direction. For a single k channel as defined in Eq. (15), this Hamiltonian is one dimensional, and hence it is possible to solve it with a similar method as that introduced in Refs. [60,61]. The procedure is very similar to that explained for this specific model in Ref. [48]. We explain below the main steps.

We express the Hamiltonian as follows:

$$H_{k} = \sum_{j} H^{a}_{kj} + H^{b}_{kj} + H^{\lambda}_{kj}, \tag{C1}$$

where the first term is

$$H^{a}_{kj} = \xi_{k}\sum_{\sigma} c^{\dagger}_{kj\sigma}c_{kj\sigma} + (\Delta_{k}c^{\dagger}_{kj\uparrow}c^{\dagger}_{-kj\downarrow} + \mathrm{H.c.}), \tag{C2}$$

and the second one is

$$H^{b}_{kj} = -t(c^{\dagger}_{kj+1\sigma}c_{kj\sigma} + \mathrm{H.c.}) + [-i\lambda(c^{\dagger}_{kj+1\uparrow}c_{kj\uparrow} - c^{\dagger}_{kj+1\downarrow}c_{kj\downarrow}) + \Delta_{1}(c^{\dagger}_{kj\uparrow}c^{\dagger}_{-kj+1\downarrow} + c^{\dagger}_{-kj+1\uparrow}c^{\dagger}_{kj\downarrow}) + \mathrm{H.c.}]. \tag{C3}$$

These two terms are combined as follows:

$$H^{0}_{k} = \sum_{j}\left(H^{a}_{kj} + H^{b}_{kj} + H^{a}_{-kj} + H^{b}_{-kj}\right), \tag{C4}$$

and this Hamiltonian is solved exactly. The third term is

$$H^{\lambda}_{kj} = -2\lambda\sin k(c^{\dagger}_{kj\uparrow}c_{kj\downarrow} + c^{\dagger}_{kj\downarrow}c_{kj\uparrow}), \tag{C5}$$

and it is treated as a perturbation, by defining

$$H^{\lambda}_{k} = \sum_{j}\left(H^{\lambda}_{kj} + H^{\lambda}_{-kj}\right). \tag{C6}$$

As in previous works [48,59], the Hamiltonian matrix is expressed in a basis constructed by mapping the annihilation (a) and creation (c) operators to different states:

$$c_{\alpha} \leftrightarrow |\alpha a\rangle, \; c^{\dagger}_{\alpha} \leftrightarrow |\alpha c\rangle. \tag{C7}$$

A solution for H^0_k in a chain of N_x sites with open boundary conditions with the structure of states of the generalized Bloch form

$$|zk\sigma b\rangle = \sum_{j=1}^{N_x} z^{j-1}|kj\sigma b\rangle, \tag{C8}$$

where $b = a$ or c, is proposed. Following the same steps as in Refs. [48,59], a zero mode localized at the left (L) side of the stripe is obtained:

$$\gamma_{Lk\uparrow} = N_{k}\sum_{i=1}^{2}\alpha_{i}\sum_{j=1}^{N_x} z_{i}^{j-1}(c_{kj\uparrow} + i\zeta c^{\dagger}_{-kj\downarrow}), \tag{C9}$$

where the (k dependent) z_i and α_i are determined by requesting that Eq. (C8) is an eigenstate of H^0_k with zero energy, which leads to a second-order polynomial in z, with roots z_1, z_2. $\zeta = \mathrm{sgn}(\lambda\Delta_1)$ has been chosen to lead to $|z_i| < 1$. The normalization factor N_k is determined from $\{\gamma_{k\uparrow}, \gamma^{\dagger}_{k\uparrow}\} = 1$,

$$N_{k}^{-2} = 2\sum_{j=1}^{N_x}\left|\sum_{i=1}^{2}\alpha_{i}z_{i}^{j-1}\right|^{2} \simeq 2\left(\sum_{i=1}^{2}\frac{|\alpha_{i}|^{2}}{1-|z_{i}|^{2}} + \frac{\alpha_{1}\bar{\alpha}_{2}}{1-z_{i}\bar{z}_{2}} + \frac{\bar{\alpha}_{1}\alpha_{2}}{1-\bar{z}_{1}z_{2}}\right), \tag{C10}$$

where in the last equality, it has been assumed that N_x is much larger than the localization length of the zero mode.

Using time-reversal symmetry, the corresponding solution for the Kramer's partner with spin down is obtained:

$$\gamma_{Lk\downarrow} = N_{k}\sum_{i=1}^{2}\bar{\alpha}_{i}\sum_{j=1}^{N_x}\bar{z}_{i}^{j-1}(c_{kj\downarrow} + i\zeta c^{\dagger}_{-kj\uparrow}), \tag{C11}$$

where we have used that N_k, α_i, and z_i are even in k. Moving the parameters, this continues to be valid by continuity until $|z_i| = 1$ is reached for one of the roots. At this point the zero mode disappears [the normalization factor in Eq. (C9) vanishes, see Eq. (C10)] and the system ceases to be topological. Note that

$$\gamma^{\dagger}_{Lk\sigma} = -i\zeta\gamma_{L-k-\sigma}. \tag{C12}$$

So far, we have obtained exactly the zero modes of the Hamiltonian disregarding H^{λ}_{k}. Using Eq. (C9), we obtain for

the complete Hamiltonian

$$[\gamma_{Lk\uparrow}, H] = (-2\lambda \sin k)N_k \sum_{i=1}^{2} \alpha_i \sum_{j=1}^{N_x} z_i^{j-1}(c_{kj\downarrow} + i\zeta c^{\dagger}_{-kj\uparrow}). \tag{C13}$$

The second member of this equation has a low-energy part proportional to $\gamma_{Lk\downarrow}$ and a high-energy part. In first-order perturbation theory in H_k^{λ} we consider only the former part, which is obtained by anticommuting the second member with $\gamma^{\dagger}_{Lk\downarrow}$. The result is

$$[\gamma_{Lk\uparrow}, H] = -2\lambda\rho_k e^{i\varphi_k} \sin k\gamma_{Lk\downarrow} + \cdots, \tag{C14}$$

where $\cdots$ denotes the high-energy part (a continuum of excited states), and ρ_k and φ_k are the modulus and phase of the complex number,

$$\begin{aligned}\rho_k e^{i\varphi_k} &= 2N_k^2 \sum_{j=1}^{N_x} \left(\sum_{i=1}^{2} \alpha_i z_i^{j-1} \right)^2 \\ &\simeq 2N_k^2 \left(\sum_{i=1}^{2} \frac{\alpha_i^2}{1 - z_i^2} + \frac{2\alpha_1\alpha_2}{1 - z_1 z_2} \right),\end{aligned} \tag{C15}$$

where in the last equality it has been assumed that N_x is much larger than the localization length of the zero mode. Note that all quantities in Eq. (C15) are even in k.

Using Eq. (C14) we obtain the eigenmodes

$$\begin{aligned}\eta_{Lk\pm} &= \frac{1}{\sqrt{2}}(\gamma_{Lk\uparrow} \pm e^{i\varphi_k}\gamma_{Lk\downarrow}),\ [\eta_{Lk\pm}, H] = \pm\varepsilon_{\lambda,k}, \\ \varepsilon_{\lambda,k} &= -2\lambda\rho_k \sin k.\end{aligned} \tag{C16}$$

Under time reversal K these operators transform as

$$K\eta_{Lk\pm}K^{\dagger} = \mp e^{-i\varphi_k}\eta_{L-k\mp}. \tag{C17}$$

Using Eq. (C12), the following property is easily proved:

$$\eta^{\dagger}_{L-k\pm} = \mp i\zeta e^{-i\varphi_k}\eta_{Lk\pm}. \tag{C18}$$

The resulting energies are in excellent agreement with numerical results for parameters well inside the topological region, for which $\rho_k \sim 1$, for example, $t = 1$, $\mu = 2$, $\Delta_0 = 4$, $\Delta_1 = 2.2$, $\lambda = 7$, and k near π. If the largest $|z_i|$ approaches 1, ρ_k is small and the results lose accuracy. The dependence of ρ_k with k is important. In general, the system is topological for small ξ_k and Δ_k [see Eq. (C2)] [31], a condition difficult to satisfy for all k, except for very small t and Δ_0.

The low-energy states with important amplitude for sites near $j = N_x$ can be obtained from those derived above by reflection (where j is interchanged with $N_x + 1 - j$) and complex conjugation (as done before [48] and confirmed numerically). Then we have

$$\begin{aligned}\gamma_{Rk\uparrow} &= N_k \sum_{i=1}^{2} \bar{\alpha}_i \sum_{j=1}^{N_x} \bar{z}_i^{N_x - j}(c_{kj\uparrow} - i\zeta c^{\dagger}_{-kj\downarrow}), \\ \gamma_{Rk\downarrow} &= N_k \sum_{i=1}^{2} \alpha_i \sum_{j=1}^{N_x} z_i^{N_x - j}(c_{kj\downarrow} - i\zeta c^{\dagger}_{-kj\uparrow}), \\ \eta_{Rk\pm} &= \frac{1}{\sqrt{2}}(\gamma_{Rk\uparrow} \pm e^{-i\varphi_k}\gamma_{Rk\downarrow}),\end{aligned} \tag{C19}$$

with the following properties similar to Eqs. (C12) and (C18):

$$\gamma^{\dagger}_{Rk\sigma} = i\zeta\gamma_{R-k-\sigma}, \quad \eta^{\dagger}_{R-k\pm} = \pm i\zeta e^{i\varphi_k}\eta_{Rk\pm}. \tag{C20}$$

APPENDIX D: DERIVATION OF THE EFFECTIVE HAMILTONIAN FOR THE TRITOPS-S JUNCTION

We consider the low-energy effective Hamiltonian for the TRITOPS (S2) in Eq. (22):

$$H_{S2} = \sum_{k>0} \varepsilon_{\lambda,k}(\eta^{\dagger}_{k+}\eta_{k+} - \eta^{\dagger}_{k-}\eta_{k-}), \tag{D1}$$

with $\varepsilon_{\lambda,k}$ given by Eq. (19). The nontopological superconductor (S) is modeled by Eq. (37). We substitute Eqs. (29) and (30) in the operators of the TRITOPS side, while for the S side we use

$$c^{\dagger}_{k\uparrow} = \frac{1}{\sqrt{2}}(d^{\dagger}_{k+} + d^{\dagger}_{k-}),\ c^{\dagger}_{k\downarrow} = \frac{1}{\sqrt{2}}(d_{-k+} - d_{-k-}). \tag{D2}$$

The effective phase-dependent tunneling Hamiltonian for the junction, obtained after adding the contributions of k and $-k$, reads

$$\begin{aligned}\frac{\sqrt{2}H_J^k}{t_J} &= \eta^{\dagger}_{Lk+}[w_k g_-(\phi)d_{k+} + w_k g_+(\phi)d_{k-} + \bar{w}_k e^{i\varphi_k} g_-(\phi)d^{\dagger}_{-k+} - \bar{w}_k e^{i\varphi_k} g_+(\phi)d^{\dagger}_{-k-}] \\ &\quad + \eta^{\dagger}_{Lk-}[w_k g_-(\phi)d_{k+} + w_k g_+(\phi)d_{k-} - \bar{w}_k e^{i\varphi_k} g_-(\phi)d^{\dagger}_{-k+} + \bar{w}_k e^{i\varphi_k} g_+(\phi)d^{\dagger}_{-k-}] + \text{H.c.},\end{aligned} \tag{D3}$$

where

$$g_{\pm}(\phi) = e^{-i\phi/2} \pm i\zeta e^{i\phi/2}. \tag{D4}$$

The fermionic degrees of freedom of S can be "integrated-out" by treating H_J^k in second order of perturbation theory. The result is the effective Hamiltonian for the TRITOPS edge given in Eq. (40).

[1] B. A. Bernevig, *Topological Insulators and Topological Superconductors* (Princeton University Press, Princeton, NJ, 2013).

[2] A. Y. Kitaev, Unpaired Majorana fermions in quantum wires, Phys. Usp. **44**, 131 (2001).

[3] M. H. Freedman, M. Larsen, and Z. Wang, A modular functor which is universal for quantum computation, Commun. Math. Phys. **227**, 605 (2002).

[4] A. Y. Kitaev, Fault-tolerant quantum computation by anyons, Ann. Phys. **303**, 2 (2003).

[5] R. M. Lutchyn, J. D. Sau, and S. DasSarma, Majorana Fermions and a Topological Phase Transition in Semiconductor-Superconductor Heterostructures, Phys. Rev. Lett. **105**, 077001 (2010).

[6] Y. Oreg, G. Refael, and F. von Oppen, Helical Liquids and Majorana Bound States in Quantum Wires, Phys. Rev. Lett. **105**, 177002 (2010).

[7] V. Mourik, K. Zuo, S. M. Frolov, S. Plissard, E. P. Bakkers, and L. P. Kouwenhoven, Signatures of Majorana fermions in hybrid superconductor-semiconductor nanowire devices, Science **336**, 1003 (2012).

[8] L. P. Rokhinson, X. Liu, and J. K. Furdyna, The fractional ac Josephson effect in a semiconductor–superconductor nanowire as a signature of Majorana particles, Nat. Phys. **8**, 795 (2012).

[9] A. Das, Y. Ronen, Y. Most, Y. Oreg, M. Heiblum, and H. Shtrikman, Zero-bias peaks and splitting in an Al-InAs nanowire topological superconductor as a signature of Majorana fermions, Nat. Phys. **8**, 887 (2012).

[10] S. M. Albrecht, A. P. Higginbotham, M. Madsen, F. Kuemmeth, T. S. Jespersen, J. Nygård, P. Krogstrup, and C. Marcus, Exponential protection of zero modes in Majorana islands, Nature (London) **531**, 206 (2016).

[11] S. Deng, L. Viola, and G. Ortiz, Majorana Modes in Time-Reversal Invariant *s*-Wave Topological Superconductors, Phys. Rev. Lett. **108**, 036803 (2012).

[12] S. Nadj-Perge, I. K. Drozdov, J. Li, H. Chen, S. Jeon, J. Seo, A. H. MacDonald, B. A. Bernevig, and A. Yazdani, Observation of Majorana fermions in ferromagnetic atomic chains on a superconductor, Science **346**, 602 (2014).

[13] H. Kim, A. Palacio-Morales, T. Posske, L. Rózsa, K. Palotás, L. Szunyogh, M. Thorwart, and R. Wiesendanger, Toward tailoring Majorana bound states in artificially constructed magnetic atom chains on elemental superconductors, Sci. Adv. **4**, eaar5251 (2018).

[14] M. Ruby, F. Pientka, Y. Peng, F. von Oppen, B. W. Heinrich, and K. J. Franke, End States and Subgap Structure in Proximity-Coupled Chains of Magnetic Adatoms, Phys. Rev. Lett. **115**, 197204 (2015).

[15] P. Zhang, K. Yaji, T. Hashimoto, Y. Ota, T. Kondo, K. Okazaki, Z. Wang, J. Wen, G. Gu, H. Ding, *et al.*, Observation of topological superconductivity on the surface of an iron-based superconductor, Science **360**, 182 (2018).

[16] L. Fu and C. L. Kane, Superconducting Proximity Effect and Majorana Fermions at the Surface of a Topological Insulator, Phys. Rev. Lett. **100**, 096407 (2008).

[17] L. Fu and C. L. Kane, Josephson current and noise at a superconductor/quantum-spin-Hall-insulator/superconductor junction, Phys. Rev. B **79**, 161408(R) (2009).

[18] X.-L. Qi and S.-C. Zhang, Topological insulators and superconductors, Rev. Mod. Phys. **83**, 1057 (2011).

[19] J. Alicea, New directions in the pursuit of Majorana fermions in solid state systems, Rep. Prog. Phys. **75**, 076501 (2012).

[20] R. Aguado, Majorana quasiparticles in condensed matter, La Rivista del Nuovo Cimento **40**, 523 (2017).

[21] K. Flensberg, F. von Oppen, and A. Stern, Engineered platforms for topological superconductivity and Majorana zero modes, Nat. Rev. Mater. **6**, 944 (2021).

[22] S. Ryu, A. P. Schnyder, A. Furusaki, and A. W. Ludwig, Topological insulators and superconductors: Tenfold way and dimensional hierarchy, New J. Phys. **12**, 065010 (2010).

[23] X.-L. Qi, T. L. Hughes, S. Raghu, and S.-C. Zhang, Time-Reversal-Invariant Topological Superconductors and Superfluids in Two and Three Dimensions, Phys. Rev. Lett. **102**, 187001 (2009).

[24] E. Dumitrescu and S. Tewari, Topological properties of the time-reversal-symmetric Kitaev chain and applications to organic superconductors, Phys. Rev. B **88**, 220505(R) (2013).

[25] A. Haim, A. Keselman, E. Berg, and Y. Oreg, Time-reversal-invariant topological superconductivity induced by repulsive interactions in quantum wires, Phys. Rev. B **89**, 220504(R) (2014).

[26] Y. Tanaka, Y. Mizuno, T. Yokoyama, K. Yada, and M. Sato, Anomalous Andreev Bound State in Noncentrosymmetric Superconductors, Phys. Rev. Lett. **105**, 097002 (2010).

[27] K. S. H. Kwon and V. Yakovenko, Fractional ac Josephson effect in p- and d-wave superconductors, Eur. Phys. J. B **37**, 349 (2003).

[28] L. Fu and E. Berg, Odd-Parity Topological Superconductors: Theory and Application to $Cu_xBi_2Se_3$, Phys. Rev. Lett. **105**, 097001 (2010).

[29] M. S. Scheurer and J. Schmalian, Topological superconductivity and unconventional pairing in oxide interfaces, Nat. Commun. **6**, 6005 (2015).

[30] C. L. M. Wong and K. T. Law, Majorana Kramers doublets in $d_{x^2-y^2}$-wave superconductors with Rashba spin-orbit coupling, Phys. Rev. B **86**, 184516 (2012).

[31] F. Zhang, C. L. Kane, and E. J. Mele, Time-Reversal-Invariant Topological Superconductivity and Majorana Kramers Pairs, Phys. Rev. Lett. **111**, 056402 (2013).

[32] A. Keselman, L. Fu, A. Stern, and E. Berg, Inducing Time-Reversal-Invariant Topological Superconductivity and Fermion Parity Pumping in Quantum Wires, Phys. Rev. Lett. **111**, 116402 (2013).

[33] A. Haim, K. Wölms, E. Berg, Y. Oreg, and K. Flensberg, Interaction-driven topological superconductivity in one dimension, Phys. Rev. B **94**, 115124 (2016).

[34] C. Reeg, C. Schrade, J. Klinovaja, and D. Loss, DIII topological superconductivity with emergent time-reversal symmetry, Phys. Rev. B **96**, 161407(R) (2017).

[35] L. Santos, T. Neupert, C. Chamon, and C. Mudry, Superconductivity on the surface of topological insulators and in two-dimensional noncentrosymmetric materials, Phys. Rev. B **81**, 184502 (2010).

[36] J. Klinovaja, A. Yacoby, and D. Loss, Kramers pairs of Majorana fermions and parafermions in fractional topological insulators, Phys. Rev. B **90**, 155447 (2014).

[37] E. Mellars and B. Béri, Signatures of time-reversal-invariant topological superconductivity in the Josephson effect, Phys. Rev. B **94**, 174508 (2016).

[38] F. Parhizgar and A. M. Black-Schaffer, Highly tunable time-reversal-invariant topological superconductivity in topological insulator thin films, Sci. Rep. **7**, 9817 (2017).

[39] O. E. Casas, L. Arrachea, W. J. Herrera, and A. L. Yeyati, Proximity induced time-reversal topological superconductivity in

Bi_2Se_3 films without phase tuning, Phys. Rev. B **99**, 161301(R) (2019).

[40] R.-X. Zhang and S. DasSarma, Intrinsic Time-Reversal-Invariant Topological Superconductivity in Thin Films of Iron-Based Superconductors, Phys. Rev. Lett. **126**, 137001 (2021).

[41] S. B. Chung, J. Horowitz, and X.-L. Qi, Time-reversal anomaly and Josephson effect in time-reversal-invariant topological superconductors, Phys. Rev. B **88**, 214514 (2013).

[42] S. Nakosai, J. C. Budich, Y. Tanaka, B. Trauzettel, and N. Nagaosa, Majorana Bound States and Nonlocal Spin Correlations in a Quantum Wire on an Unconventional Superconductor, Phys. Rev. Lett. **110**, 117002 (2013).

[43] C. Schrade, A. A. Zyuzin, J. Klinovaja, and D. Loss, Proximity-Induced π Josephson Junctions in Topological Insulators and Kramers Pairs of Majorana Fermions, Phys. Rev. Lett. **115**, 237001 (2015).

[44] J. Li, W. Pan, B. A. Bernevig, and R. M. Lutchyn, Detection of Majorana Kramers Pairs Using a Quantum Point Contact, Phys. Rev. Lett. **117**, 046804 (2016).

[45] C. Knapp, A. Chew, and J. Alicea, Fragility of the Fractional Josephson Effect in Time-Reversal-Invariant Topological Superconductors, Phys. Rev. Lett. **125**, 207002 (2020).

[46] A. Camjayi, L. Arrachea, A. Aligia, and F. von Oppen, Fractional Spin and Josephson Effect in Time-Reversal-Invariant Topological Superconductors, Phys. Rev. Lett. **119**, 046801 (2017).

[47] C. Schrade and L. Fu, Parity-Controlled 2π Josephson Effect Mediated by Majorana Kramers Pairs, Phys. Rev. Lett. **120**, 267002 (2018).

[48] A. A. Aligia and L. Arrachea, Entangled end states with fractionalized spin projection in a time-reversal-invariant topological superconducting wire, Phys. Rev. B **98**, 174507 (2018).

[49] A. Haim and Y. Oreg, Time-reversal-invariant topological superconductivity in one and two dimensions, Phys. Rep. **825**, 1 (2019).

[50] W.-J. Gong, Z. Gao, W.-F. Shan, and G.-Y. Yi, Influence of an embedded quantum dot on the Josephson effect in the topological superconducting junction with Majorana doublets, Sci. Rep. **6**, 1 (2016).

[51] M. Mashkoori, A. G. Moghaddam, M. H. Hajibabaee, A. M. Black-Schaffer, and F. Parhizgar, Impact of topology on the impurity effects in extended s-wave superconductors with spin-orbit coupling, Phys. Rev. B **99**, 014508 (2019).

[52] L. Lauke, M. S. Scheurer, A. Poenicke, and J. Schmalian, Friedel oscillations and Majorana zero modes in inhomogeneous superconductors, Phys. Rev. B **98**, 134502 (2018).

[53] L. Arrachea, A. Camjayi, A. A. Aligia, and L. Gruñeiro, Catalog of Andreev spectra and Josephson effects in structures with time-reversal-invariant topological superconductor wires, Phys. Rev. B **99**, 085431 (2019).

[54] A. Haim, Spontaneous Josephson π junctions with topological superconductors, Phys. Rev. B **100**, 064505 (2019).

[55] K. Matano, M. Kriener, K. Segawa, Y. Ando, and G.-q. Zheng, Spin-rotation symmetry breaking in the superconducting state of $Cu_xBi_2Se_3$, Nat. Phys. **12**, 852 (2016).

[56] S. Yonezawa, K. Tajiri, S. Nakata, Y. Nagai, Z. Wang, K. Segawa, Y. Ando, and Y. Maeno, Thermodynamic evidence for nematic superconductivity in $Cu_xBi_2Se_3$, Nat. Phys. **13**, 123 (2017).

[57] D. Vollhardt and P. Wolfle, *The Superfluid Phases of Helium 3* (Courier Corporation, North Chelmsford, MA, 2013).

[58] N. Read and D. Green, Paired states of fermions in two dimensions with breaking of parity and time-reversal symmetries and the fractional quantum Hall effect, Phys. Rev. B **61**, 10267 (2000).

[59] A. A. Aligia, D. Perez Daroca, and L. Arrachea, Tomography of Zero-Energy End Modes in Topological Superconducting Wires, Phys. Rev. Lett. **125**, 256801 (2020).

[60] A. Alase, E. Cobanera, G. Ortiz, and L. Viola, Exact Solution of Quadratic Fermionic Hamiltonians for Arbitrary Boundary Conditions, Phys. Rev. Lett. **117**, 076804 (2016).

[61] A. Alase, E. Cobanera, G. Ortiz, and L. Viola, Generalization of Bloch's theorem for arbitrary boundary conditions: Theory, Phys. Rev. B **96**, 195133 (2017).

[62] A. A. Aligia and A. Camjayi, Exact analytical solution of a time-reversal-invariant topological superconducting wire, Phys. Rev. B **100**, 115413 (2019).

[63] Y. Tanaka and S. Kashiwaya, Theory of the Josephson effect in d-wave superconductors, Phys. Rev. B **53**, R11957 (1996).

[64] Y. Tanaka and S. Kashiwaya, Theory of Josephson effects in anisotropic superconductors, Phys. Rev. B **56**, 892 (1997).

[65] S. Kashiwaya and Y. Tanaka, Tunnelling effects on surface bound states in unconventional superconductors, Rep. Prog. Phys. **63**, 1641 (2000).

[66] M. Alidoust, M. Willatzen, and A.-P. Jauho, Strain-engineered Majorana zero energy modes and φ_0 Josephson state in black phosphorus, Phys. Rev. B **98**, 085414 (2018).

[67] M. Alidoust, Critical supercurrent and φ_0 state for probing a persistent spin helix, Phys. Rev. B **101**, 155123 (2020).

[68] M. Alidoust, C. Shen, and I. Žutić, Cubic spin-orbit coupling and anomalous Josephson effect in planar junctions, Phys. Rev. B **103**, L060503 (2021).

[69] A. Zazunov, R. Egger, T. Jonckheere, and T. Martin, Anomalous Josephson Current through a Spin-Orbit Coupled Quantum Dot, Phys. Rev. Lett. **103**, 147004 (2009).